ARO 16106.2-A-EL

(11)

Final Technical Report

DISCRIMINATION BETWEEN TARGETS AND CLUTTER BY RADAR

Authors:

J. D. Echard
E. E. Martin
D. L. Odom
H. G. Cox

Prepared for

U. S. ARMY RESEARCH OFFICE
P. O. Box 12211
Research Triangle Park, North Carolina 27709

Under

Contract No. DAAG29-78-C-0044

December 1981

GEORGIA INSTITUTE OF TECHNOLOGY
A Unit of the University System of Georgia
Engineering Experiment Station
Atlanta, Georgia 30332

GTEES

UNCLASSIFIED

SECURITY CLASSIFICATION OF THIS PAGE (When Data Entered)

REPORT DOCUMENTATION PAGE		READ INSTRUCTIONS BEFORE COMPLETING FORM
1. REPORT NUMBER	2. GOVT ACCESSION NO. AD-A111 583	3. RECIPIENT'S CATALOG NUMBER
4. TITLE (and Subtitle) DISCRIMINATION BETWEEN TARGETS AND CLUTTER BY RADAR		5. TYPE OF REPORT & PERIOD COVERED Final Report Sept. 20, 1978-Sept. 19, 1981
		6. PERFORMING ORG. REPORT NUMBER GIT/EES - A-2230 FTR
7. AUTHOR(s) J. D. Echard, E. E. Martin, D. L. Odom, and H. G. Cox		8. CONTRACT OR GRANT NUMBER(s) DAAG29-78-C-0044
9. PERFORMING ORGANIZATION NAME AND ADDRESS Georgia Institute of Technology Engineering Experiment Station Atlanta, Georgia 30332		10. PROGRAM ELEMENT, PROJECT, TASK AREA & WORK UNIT NUMBERS
11. CONTROLLING OFFICE NAME AND ADDRESS U. S. Army Research Office Post Office Box 12211 Research Triangle Park, NC 27709		12. REPORT DATE December 1981
		13. NUMBER OF PAGES 66
14. MONITORING AGENCY NAME & ADDRESS (if different from Controlling Office) U.S. Army Electronic Research and Development Command (DELCS-R-M) Fort Monmouth, New Jersey 07703		15. SECURITY CLASS. (of this report) Unclassified
		15a. DECLASSIFICATION/DOWNGRADING SCHEDULE

16. DISTRIBUTION STATEMENT (of this Report)

Approved for public release; distribution unlimited.

17. DISTRIBUTION STATEMENT (of the abstract entered in Block 20, if different from Report)

NA

18. SUPPLEMENTARY NOTES

The view, opinions, and/or findings contained in this report are those of the author(s) and should not be construed as an official Department of the Army position, policy, or decision, unless so designated by other documentation.

19. KEY WORDS (Continue on reverse side if necessary and identify by block number)

Radar
Radar Discrimination
Stationary Target Detection

20. ABSTRACT (Continue on reverse side if necessary and identify by block number)

A study of the discrimination of military targets by radar performed from September 20, 1978 through September 19, 1981 is summarized in this report. The overall objective of the study was to analyze and synthesize radar signal processing techniques towards the design of a practical radar system with stationary weapons as the primary target.

The discrimination techniques irvestigated utilizes both frequency agility and polarization information. The performance of several Pseudo-Coherent Detection

DD FORM 1 JAN 73 1473 EDITION OF 1 NOV 65 IS OBSOLETE

UNCLASSIFIED

SECURITY CLASSIFICATION OF THIS PAGE (When Data Entered)

20. Abstract (continued)

(PCD) algorithms are compared to square-law detection with a constant false alarm rate (CFAR) processor. Intracell and intercell performance of these discrimination processors are determined using theoretical analyses.

DISCRIMINATION BETWEEN TARGETS AND CLUTTER BY RADAR

Final Technical Report

Authors:

J. D. Echard
E. E. Martin,
D. L. Odom, and
H. G. Cox

December 1981

U. S. Army Research Office
Post Office Box 12211
Research Triangle Park, North Carolina 27709

Contract No. DAAG29-78-C-0044

Georgia Institute of Technology
Engineering Experiment Station
Atlanta, Georgia 30332

THE VIEW, OPINIONS, AND/OR FINDINGS CONTAINED IN THIS REPORT ARE THOSE OF THE AUTHOR(S) AND SHOULD NOT BE CONSTRUED AS AN OFFICIAL DEPARTMENT OF THE ARMY POSITION, POLICY, OR DECISION, UNLESS SO DESIGNATED BY OTHER DOCUMENTATION.

TABLE OF CONTENTS

LIST OF ILLUSTRATIONS

LIST OF ILLUSTRATIONS

(continued)

LIST OF TABLES

FOREWARD

The research on this program was conducted by the Radar Applications Division, Radar and Instrumentation Laboratory, Engineering Experiment Station, Georgia Institute of Technology, Atlanta, Georgia, with Dr. J. D. Echard serving as Project Director and Mr. E. E. Martin serving as Associate Project Director.

This report was prepered by the Engineering Experiment Station at the Georgia Institute of Technology for the U. S. Army Research Office under Contract DAAK29-78-C-0044. The funding was provided by the U. S. Army Electronics Research and Development Command. The Technical Monitors were Dr. B. Gelernter and Mr. W. Johnson. For the purposes of internal control at Georgia Tech, the effort was designated Project A-2230. The final report summarizes the work performed under this contract. This report covers work which was performed form September 20, 1978 through September 19, 1981.

The authors are grateful to Mr. Jim Andrews of U. S. Army, Aberdeen Proving Ground, Maryland, for his support in the Aberdeen radar measurement program. He provided personnel and assistance for the operation of the target positioner, motor-generator power suppy and cranes. In addition, appreciation is expressed to personnel from U. S. Army ERADCOM for supplying and erecting the test towers and building used in this measurement program.

The guidance of Dr. E. K. Reedy, and Mr. J. L. Eaves, Director and Associate Director, respectively, of the Radar and Instrumentation Laboratory is appreciated. Our final appreciation goes to the Radar Applications Division Secretaries, Ms. Deborah Weaver and Mrs. Sandra Saxon, who typed this report.

THIS PAGE IS INTENTIONALLY LEFT BLANK

SECTION 1
INTRODUCTION AND STATEMENT OF PROBLEM

In order to optimize the effectiveness of expensive weapons, it is essential for intelligence-gathering systems to not only detect and locate potential targets, but also to properly identify those targets that are of interest. As a result, the accurate identification of military targets has been a subject of great interest in recent years. The emphasis has mainly been on solving the problems associated with separating target returns from noise and background clutter interference, and with the subsequent identification of those targets that are of interest.

The Georgia Institute of Technology, Engineering Experiment Station (GIT/EES) has been actively engaged in studies to identify stationary, military targets by radar [1-15]. The overall objective has been to analyze and synthesize radar signal processing techniques for application aboard an airborne platform with stationary, tactical weapons as primary targets. The present report contains the unclassified results of target discrimination efforts conducted by GIT/EES during the period from September 20, 1978 through December 19, 1981; the research program is under sponsorship of the U. S. Army Electronics Research and Development Command (USA ERADCOM) through the U. S. Army Research Office under Contract Number DAAG29-78-C-0044.

In order to better understand this report, it would be worthwhile to briefly consider the process of identifying a target. Referring to Figure 1.1, the identification process may be viewed as a sequence of three steps: the detection, discrimination, and classification stages. The detection process is a relatively simple one and is designed to identify all radar resolution cells in the search area which contain potential targets while keeping the number of false alarms from clutter and, primarily, from noise at a relatively small level (the probability of false alarm per cell is typically 10^{-5} or less). Since the number of cells which must be investigated is large, the detection procedure should be relatively simple and fast; the techniques employed for this purpose are well known and will not be discussed in this report. The second step in the identification process, the discrimination stage, provides a further attempt at reducing the number of false alarms. For this purpose, efforts have been directed toward the use of techniques which exploit discriminants such as those that may result from frequency agility, from utilization of polarization, or both. The final step in the identification process, the

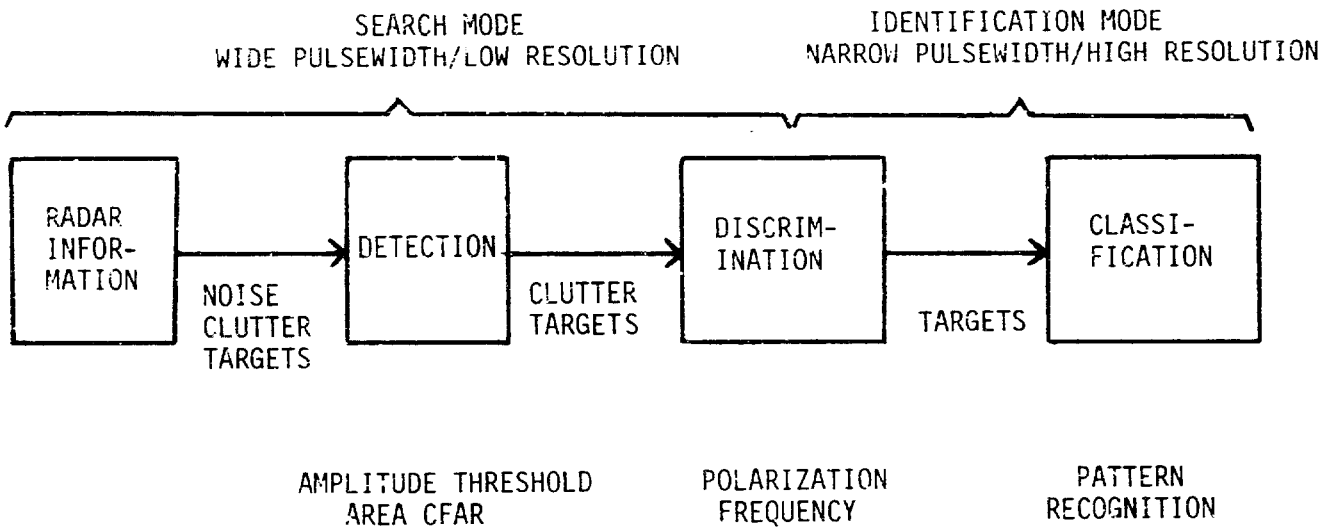

Figure 1.1 Identification process.

classification stage, consists of making a decision with respect to the identity of the target by assigning it to one of various possible categories.

Results of a theoretical study to determine the performance of one particular class of discrimination algorithms utilizing polarimetric information is presented in this report. Two types of pseudo-coherent detection (PCD) processors which utilize polarimetric phase, the relative phase between the horizontally and vertically polarized received signals, were analyzed and their performance determined.

Also X-band and 95 GHz radar data were collected on five military targets under this contract to be used in a computer simulation of polarimetric detection processors. A description of the data collected and the system used to collect the data is given in this report. However, the interpretation and processing of this data will be performed under a later contract.

THIS PAGE IS INTENTIONALLY LEFT BLANK

SECTION 2
TARGET-CLUTTER DISCRIMINATION

2.1 INTRODUCTION

A discrimination processor is the heart of any radar system which must detect and classify targets in a background of clutter and noise. The discrimination processing can be more complex and time consuming than that associated with detection processing, since the detection processor will have reduced the cells requiring further investigation to a small percentage of the total number of cells in the search area. In general, the false detection (false threat indication) probability does not have to be as small for discrimination as it is for detection. However, because of the importance of detecting threat targets, the false dismissal probability should be low. Since it is extremely difficult to find a single discriminant which will provide superior performance over a wide variety of target and environmental conditions, it may be necessary to combine the outputs of several discriminants to obtain a satisfactory target/clutter decision. Each discriminant should take advantage of known differences in scattering characteristics between targets and clutter.

The radar sensor can measure the amplitude, time delay, frequency (Doppler) and phase of the scattered signal as functions of time. If the operational situation allows, amplitude, phase and Doppler may also be measured as functions of frequency, aspect angle and polarization. Most discriminants operate on one or more of the variables mentioned above. Considering the problem of detecting stationary targets, it is apparent that Doppler discriminants are not applicable. Also, it is assumed that discrimination will be performed on the data collected in the search (or detection) mode. These data will probably have low resolution with respect to the target dimensions so that individual target scattering centers will not be resolved. Thus time delay does not appear to be a viable dimension for discrimination. However, we are left with the amplitude and phase of the scattered radar signal as functions of time, polarization, aspect angle and possibly frequency as the quantities to be used for discrimination.

In this study, combinations of amplitude and polarimetric phase, the relative phase between the horizontally and vertically polarized received signals, were investigated for discrimination capability. Results of studies to determine the performance of one particular discrimination algorithm called Pseudo-Coherent Detection (PCD) are

presented. Since the PCD-phase only processor is a single range cell constant false alarm process, a distinction between its performance in a single cell and in a multiple range cell scenario must be made. Thus, a theoretical analysis of PCD in a single range cell scenario (intracell) is first addressed, and then the theoretical performance of PCD in a non-uniformly, range distributed clutter scenario involving multiple cells is determined. This latter type of performance may be thought of as intercell performance. In both of these analyses, the performance of conventional square-law, single polarization channel, detection is used as a reference.

In addition, data collected at Aberdeen Proving Ground, Maryland under this contract are described in the last section of this chapter. However, an interpretation of these measured data will not be presented in this report.

2.2 INTRACELL THEORETICAL PERFORMANCE OF PSEUDO-COHERENT DETECTION

The theoretical performance of the PCD algorithm in a single cell (intracell) scenario will now be addressed. The block diagrams of the two particular PCD algorithms under consideration in this section are shown in Figures 2.1 and 2.2. In Figure 2.1, the IF signals in the horizontally (H) and vertically (V) polarized receive channels are mixed together. Since they are at the same IF frequency, a video signal appears at the mixer output which can be represented as

$$v(t) = H(t) \cdot V(t) \sin(\theta(t)) \tag{2-1}$$

where

$$\theta(t) = \phi_H(t) - \phi_V(t) \tag{2-2}$$

The video signal can thus be thought of as the "dot-product" of the H and V signal vectors, $H \angle \phi_H$ and $V \angle \phi_V$. This implementation shall be referred to hereafter as the pseudo-coherent detector/dot product. Since phase information is utilized in this detector even though the radar may be non-coherent, this processing technique is called pseudo-coherent.

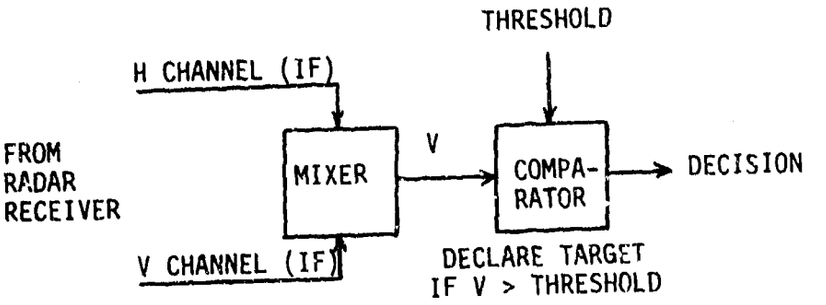

Figure 2.1 Pseudo-Coherent Detection-Dot Product algorithm implementation.

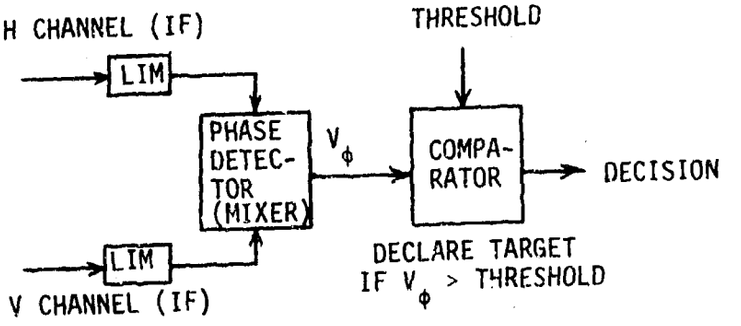

Figure 2.2 Pseudo-Coherent Detection-Phase Only algorithm implementation.

In Figure 2.2, a second PCD algorithm is shown. In this implementation the horizontally (H) and vertically (V) polarized received signals are each limited in amplitude and are submitted to a balanced mixer. In effect, the limiters and mixer perform phase detection. However, the phase detected is the relative phase between the H and V receive channels, not the absolute phase of each channel. The mixer output voltage, which is proportional to the sine of this relative phase, is subsequently submitted to a threshold and a decision is made relative to a target present or not present. This relative phase shall subsequently be referred to as polarimetric phase.

Equations describing the probability density functions of the video signal, V(t), for each of these PCD algorithms have been derived from basic assumptions and are presented here. The mathematical details are provided in Appendix A. The assumptions made are as follows:

constant amplitude (non-fluctuating) target,
clutter signals in H and V receive channels are uncorrelated,
clutter is Rayleigh distributed, and
target-plus-clutter is Ricean distributed.

For the dot product case, the probability density function was not easily derivable. However, its Fourier Transform, called the characteristic equation, was derived and is as follows:

$$c(\omega) = \frac{\mathrm{Exp}\left\{(j\omega\rho)/(1+\omega^2/4)\right\} \cdot \mathrm{Exp}\left\{(-\rho^2\omega^2)/(1+\omega^2/4)\right\}}{(1+\omega^2/4)} \qquad (2\text{-}3)$$

Where

ρ is voltage target-to-clutter ratio, $\sqrt{A^2/2\,\sigma_c^2}$, and ω is dependent variable of the equation (not frequency).

In general, the discrete inverse Fourier transform was used to determine the corresponding probability density function. This was accomplished on the computer utilizing the fast Fourier transform (FFT) for each different value of target-to-clutter

ratio, ρ . Plots of the clutter-only and target-plus-clutter densities are given in Figure 2.3 for several different values of ρ.

For some special conditions, the probability density function is derivable in closed form. For example, if the target-to-clutter ratio is zero (clutter-only), then the density function is

$$f(v) = \frac{\mathrm{Exp}\left[-|v|/\sigma_c^2\right]}{2\sigma_c^2} \quad ; \quad -\infty \leq v \leq \infty \tag{2-4a}$$

where v is the video voltage out of the mixer in Figure 2.1 and σ_c^2 is the clutter power. The clutter-only density function shown in Figure 2.3 was derived by use of the Fourier Transform but is also described by Equation (2-4a). The proper threshold for a given probability of false alarm (PFA) can be determined from Equation (2-4a) if the clutter power (σ_c^2) is known as follows:

$$v_T = -\sigma_c^2 \mathrm{Log}_e(2 \cdot PFA) \tag{2-4b}$$

Utilizing the probability density functions derived as described above, probability of detection as a function of target-to-clutter ratio (TCR) was calculated for a fixed threshold level. The results are presented in Figure 2.4 with the curve designated N=1. The effect of pulse-to-pulse integration was also determined where the clutter component for each pulse was assumed to be statistically independent. This was accomplished mathematically by convolving the proper probability density functions numerically on the computer to obtain the integrated density function. The resulting detection performance is shown in Figure 2.4 for N = 1 to 32, where N is the number of pulses integrated.

The performance of the dot product detector is also shown in another way in Figure 2.5. Here, the TCR required for a 90% detection probability and a 10^{-4} false alarm probability is shown versus the number of pulses integrated, N.

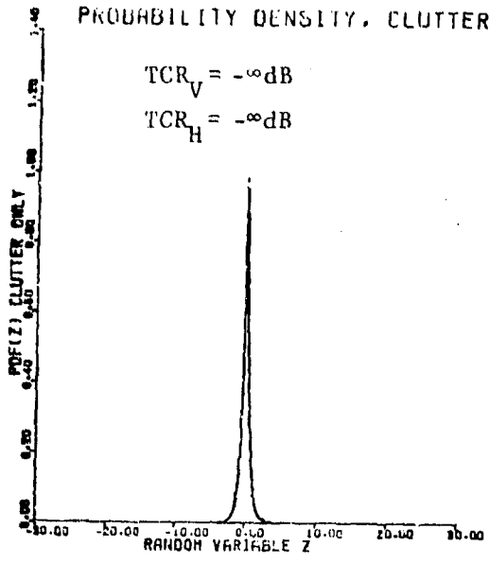

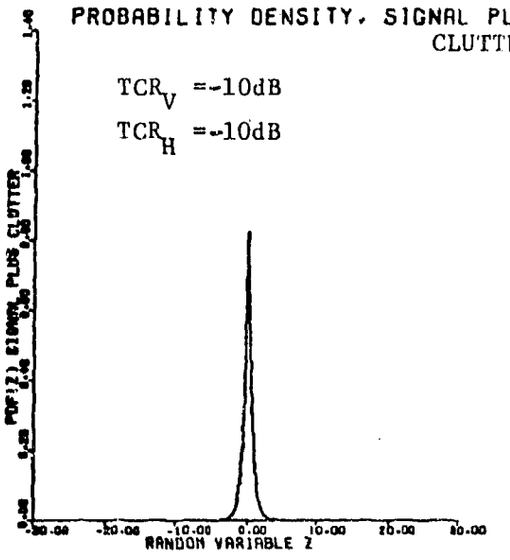

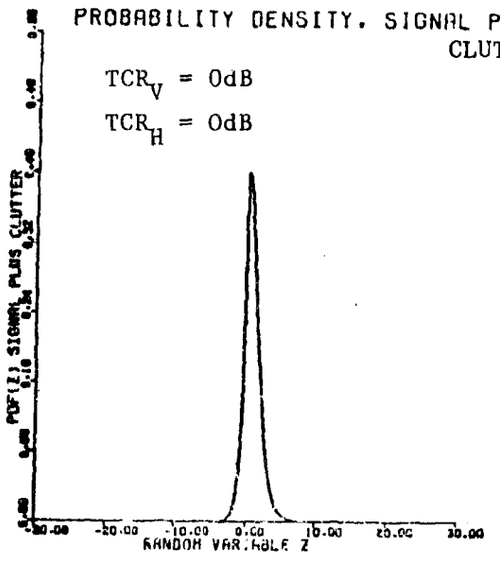

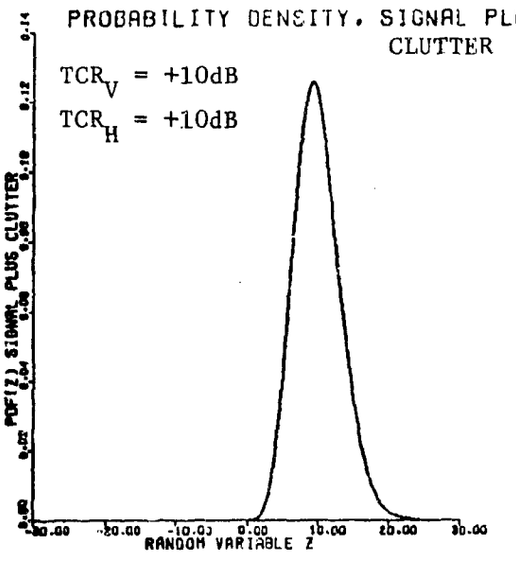

Figure 2.3 Probability density functions of voltage out of PDC-Dot Product Detector for various target-to-clutter ratios (TCR).

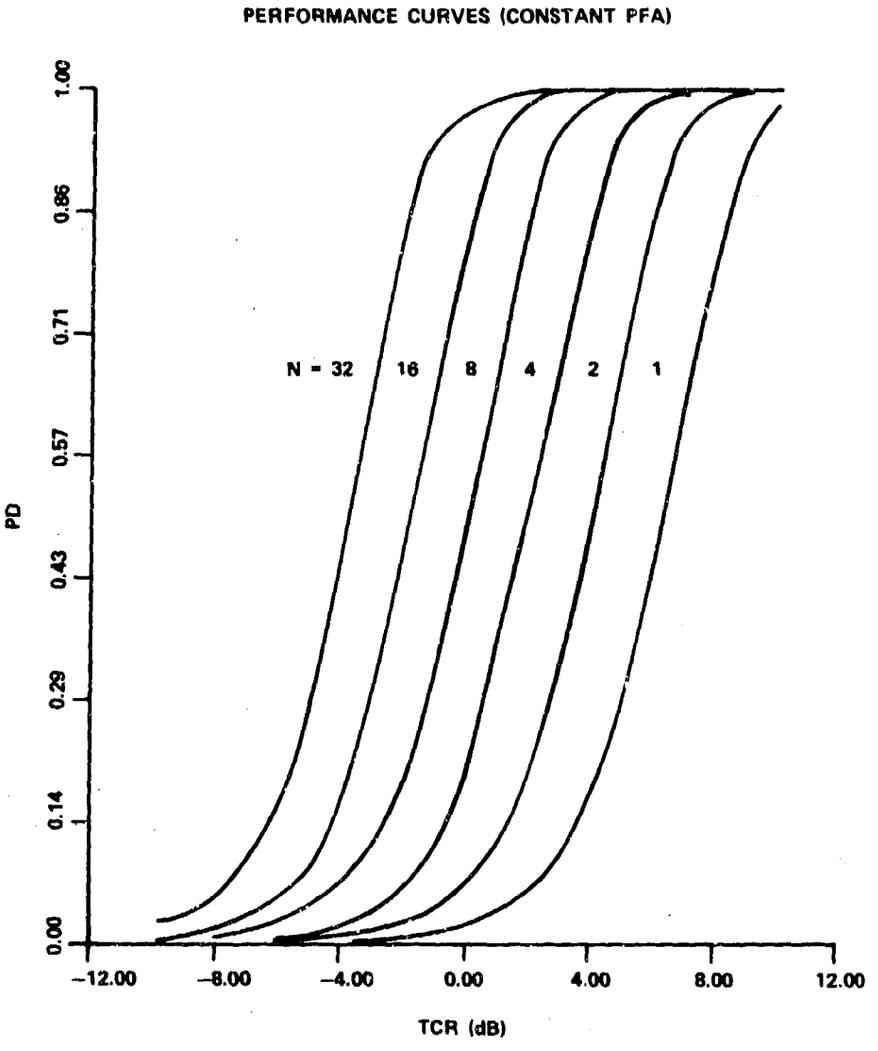

Figure 2.4 Detection performance curves for PCD-Dot Product Detector (ideal threshold setting). N = number statistically independent pulses integrated, PFA = 10^{-4}.

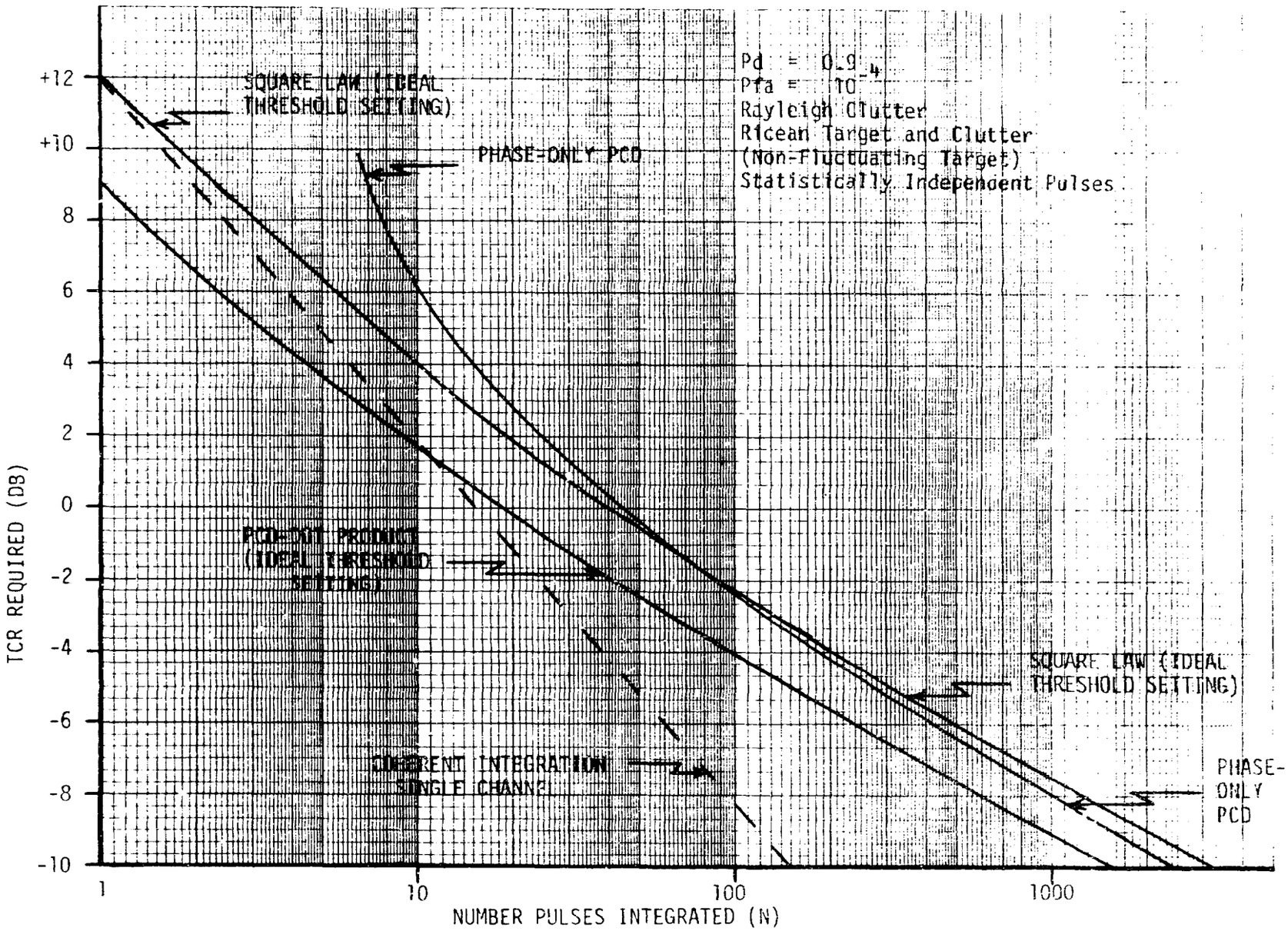

Figure 2.5 Comparative detection performance of three types of detectors. TCR required versus number of statistically independent pulses integrated. $P_D = 0.9$, $P_{FA} = 10^{-4}$.

The detection performance of the PCD-phase only has also been determined. Equations describing the probability density function of the video voltage, V(t), out of the phase-detector shown in Figure 2.2 were derived for two types of clutter-only phase distributions. These will be described in the following discussion. It is assumed that a circularly polarized wave is transmitted; however, other transmit polarizations may also be used with this type of detector.

If clutter-only is present in a range cell, and if the clutter consists of many approximately equal-sized scatterers, theoretically the polarimetric phase should be uniformly distributed and sin ϕ would be distributed as shown in Figure 2.6 (a). On the other hand, if the object in the range cell consists of only one point-source reflector such as a metal plate, corner reflector, or the like, the polarimetric phase should be concentrated near $\pm 90^{o}$ or a sin ϕ value of ± 1.

In the data collected as described in Section 2.4, the polarimetric phase does not appear to be uniformly distributed for clutter, but appears to favor phase values near zero degrees. Therefore, a more general mathematical model was derived to simulate this observed tendency as well as uniformly distributed clutter phase. It is presented in the following paragraphs.

The following single pulse probability density function for uniformly distributed polarimetric phase was derived assuming a Rayleigh distributed clutter (amplitude) model and a Ricean distributed target-plus-clutter (amplitude) model. In addition, the clutter in the H and V channels were assumed to be statistically independent.

$$f_1(Z) = \frac{1}{\pi\sqrt{1-Z^2}} \left[1 + 2 \cdot \sum_{n=1}^{\infty} A_n \cdot B_n \cdot \cos(n\cos^{-1}Z) \right]; \qquad (2\text{-}5)$$

$$-1 \leq Z \leq +1$$

Where

$$A_n = \frac{\Gamma(\frac{n}{2}+1)\rho_H^{n/2}\mathrm{Exp}(-\rho_H)}{\Gamma(n+1)} \; M(\tfrac{n}{2}+1, n+1, \rho_H)$$

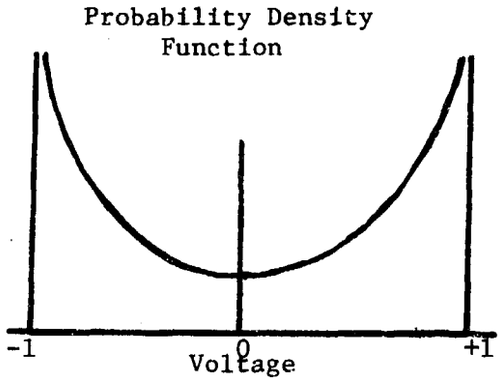

(a) Uniformly Distributed Polarimetric Phase.

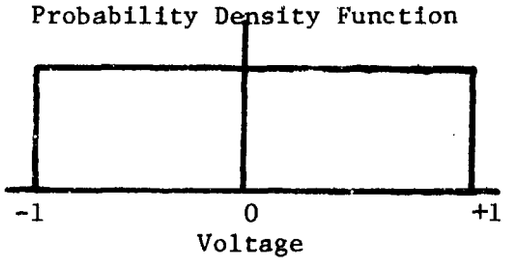

(b) Non-Uniformly Distributed Polarimetric Phase. Shape Factor is Unity.

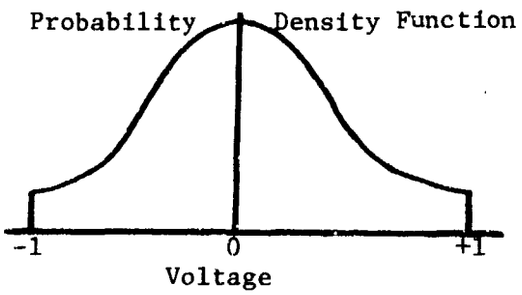

(c) Non-Uniformly Distributed Polarimetric Phase. Shape Factor is 0.25.

Figure 2.6 Mathematical Models of Clutter Probability Density Functions

$$B_n = \frac{\Gamma(\frac{n}{2}+1)\rho_V^{n/2}\,\mathrm{Exp}(-\rho_V)}{\Gamma(n+1)}\, M(\tfrac{n}{2}+1, n+1, \rho_V)$$

and where

Z is the voltage out of phase detector,

f_1 denotes single-pulse probability density function,

M(a, b, c) is the confluent hypergeometric function,

ρ_V is the voltage signal-to-clutter ratio in the vertically polarized receive channel, and

ρ_H is the voltage signal-to-clutter ratio in the horizontally polarized receive channel.

When the target-to-clutter ratio in both receive channels is zero, this probability density function becomes

$$f_1(Z) = \frac{1}{\pi\sqrt{1-Z^2}} \quad ; \quad -1 \leq Z \leq +1 \tag{2-6}$$

and describes the density function shown in Figure 2.6 (a). Plots of the density function described by Equation (2-5) for several values of target-to-clutter ratio is shown in Figure 2.7. Density functions for pulse-to-pulse integration following the PCD-phase only algorithm were obtained by mathematically convolving the appropriate density function with itself. For a large number of pulse integrations, the density function tends to be Gaussian. Probability of detection was numerically calculated and is plotted versus target-to-clutter ratio in Figure 2.8. The required target-to-clutter ratio for a PD of 90% and a PFA of 10^{-4} is plotted versus the number of pulses integrated in Figure 2.5. An interpretation of these results will be given later in this section.

For the non-uniformly distributed phase model, the following probability density function was derived for the same assumptions as before.

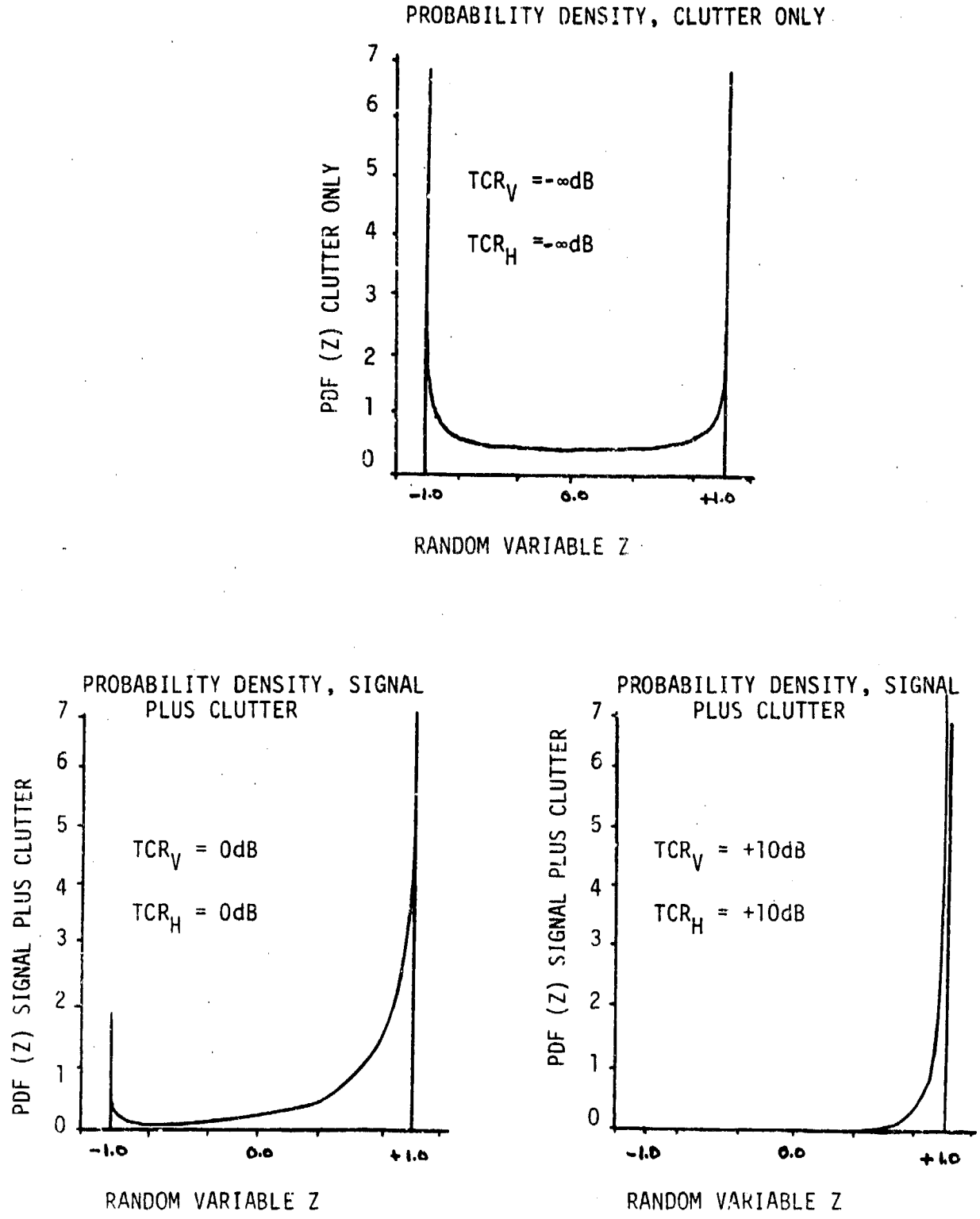

Figure 2.7 Probability density functions of voltage out of the PCD - Phase Only Detector for various target-to-clutter ratios (TCR). Uniformly distributed polarimetric phase assumed.

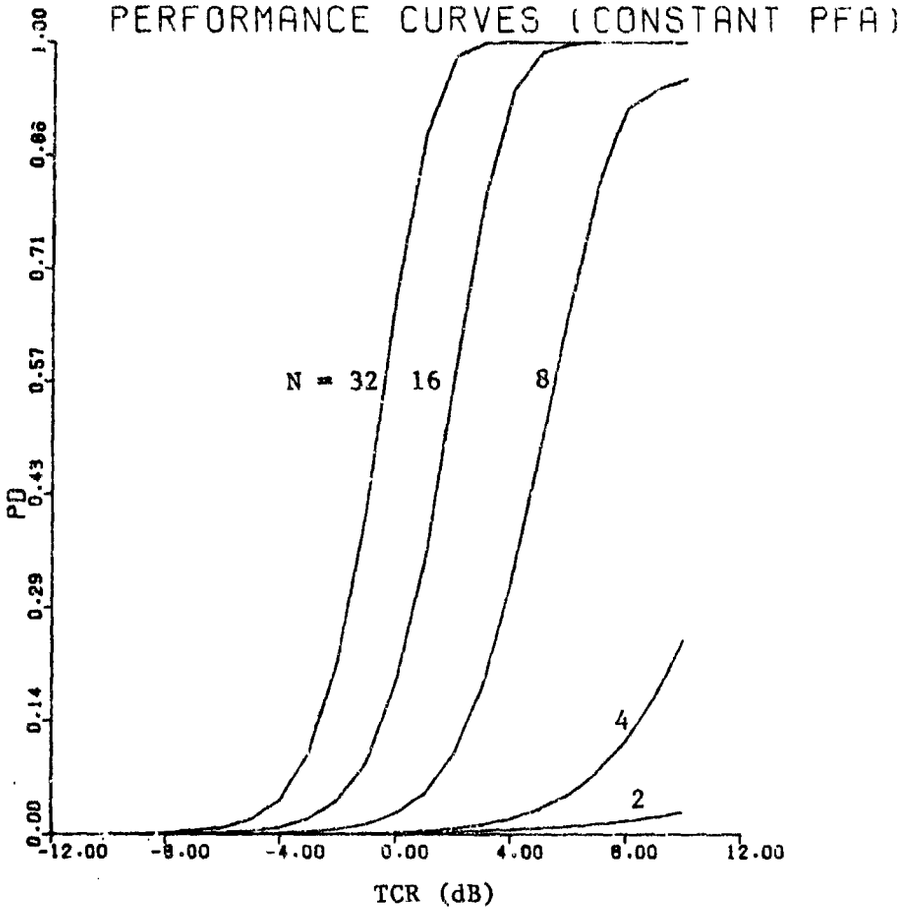

Figure 2.8 Detection performance curves for PCD-Phase Only Detector (ideal threshold setting). N = number statistically independent pulses integrated, PFA = $^{-4}$.

$$f_1(Z) = \int_{\infty}^{\infty} f_\phi(\phi_H) \cdot f_\phi(\phi_V + \lambda)\, d\lambda \tag{2-7}$$

Where

$$f_\phi(\phi) = \sec^2\phi \left[\frac{C\ \mathrm{Exp}(-\rho^2)}{\pi(C^2 + \tan^2\phi)} + \right. \tag{2-8}$$

$$+ \frac{C^2\rho\ \mathrm{Exp}\left[-\rho^2 \tan^2\phi/(C^2+\tan^2\phi)\right]}{\sqrt{\pi}\ (C^2+\tan^2\phi)^{3/2}} \left[1+\mathrm{ERF}\left[\frac{C\rho}{\sqrt{C^2+\tan^2\phi}}\right]\right] \Bigg/$$

$$\left. \left[1+\mathrm{ERF}(\rho)\right] \right]$$

and where

Z is the voltage out of phase detector,

$f_1(Z)$ is the single-pulse probability density function,

ρ is the target-to-clutter ratio either in the H or V channel,

C is a density shape factor, and

ERF ( ) is the probability error function.

Equation (2-7) represents the convolution of two phase functions and provides the density function for the voltage out of a linear phase detector;

$$Z = \phi_H - \phi_V \tag{2-9}$$

The probability density functions of ϕ_H and ϕ_V are given by Equation (2-8). The target-to-clutter ratio (ρ) in this equation is that in the H receive channel when $f_\phi(\phi_H)$ is utilized in Equation (2-7) and is that in the V receive channel when $f_\phi(\phi_V)$ is used in the equation. The density shape factor, C, is used to determine the shape of the clutter density function as illustrated in Figure 2.6. Probability density functions derived utilizing Equations (2-7) and (2-8) for several values of target-to-clutter ratio are shown in Figure 2.9 where a shape factor of unity was selected. Pulse-to-pulse integration detection performance was obtained by convolving the respective density functions as described earlier.

Detection performance for density shape factors other than unity was also derived. Interestingly, the detection performance obtained for all shape factors was identical to that obtained with the uniformly distributed polarimetric phase. After a close examination of the equations utilized, it was found that the degree of shape imparted to the clutter density function was also imparted to the target-plus-clutter density function. Thus, for a given threshold setting the relative areas under the clutter-only and target-plus-clutter probability density functions did not vary with the shape factor. In other words, the transformation being applied to obtain the desired clutter density function distribution also changed the shape of the target-to-clutter density function to the same degree. Therefore, the detection performance for all modeled clutter distributions is given by the PCD-phase only detector curves in Figures 2.5 and 2.8.

Equations for the probability density functions of the voltage out of a square-law detector were utilized with the computer to obtain the detection performance curves shown in Figure 2.11. Plots of the density function obtained are shown in Figure 2.10 for several values of target-to-clutter ratio. The purpose of generating these curves was to provide a reference to which the polarimetric processor could be compared. Also, these square-law detector results provided validation of our computer calculation procedures.

A comparison of the PCD-dot product, PCD-phase only and square-law detection performances is given in Figure 2.5. For a PD of 90% and a PFA of 10^{-4}, the required TCR versus number of pulses integrated is shown. One notes that the PCD-dot product processor requires from 1.6 dB to 3 dB less TCR than the square-law detector; the result of having an additional channel of information. The PCD-phase only and the square-law detectors have equivalent detection performance for an integration of 60 pulses or more. However, the PCD-phase only detector performance is not as good for less than

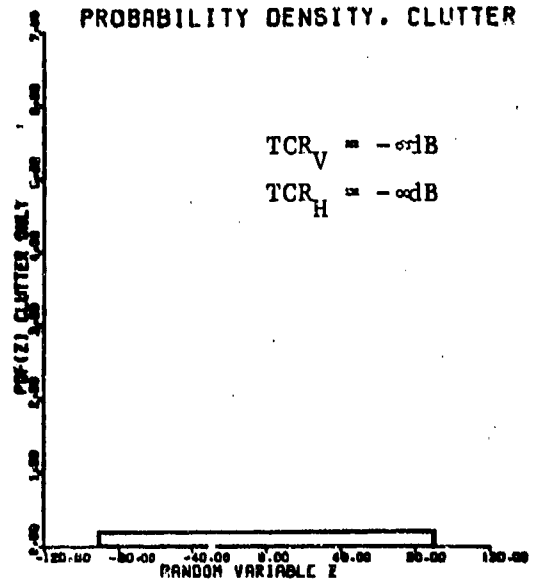

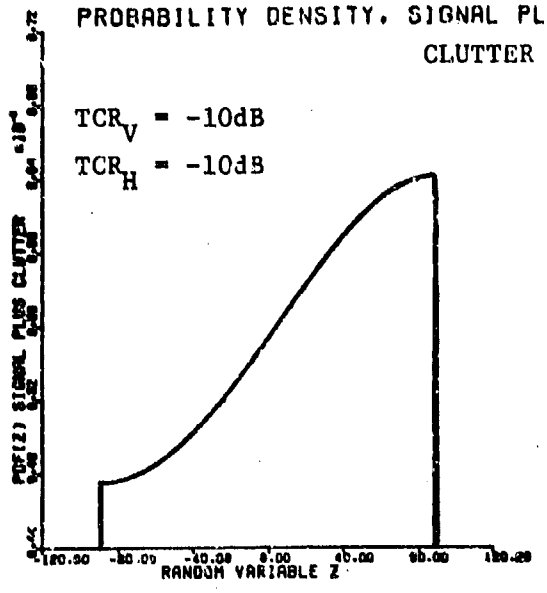

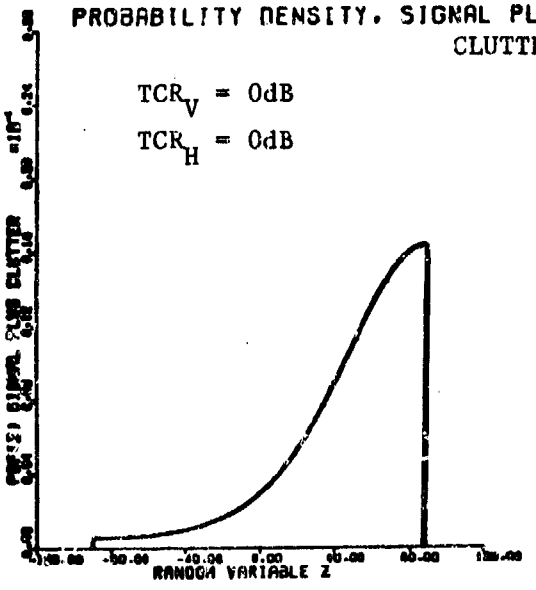

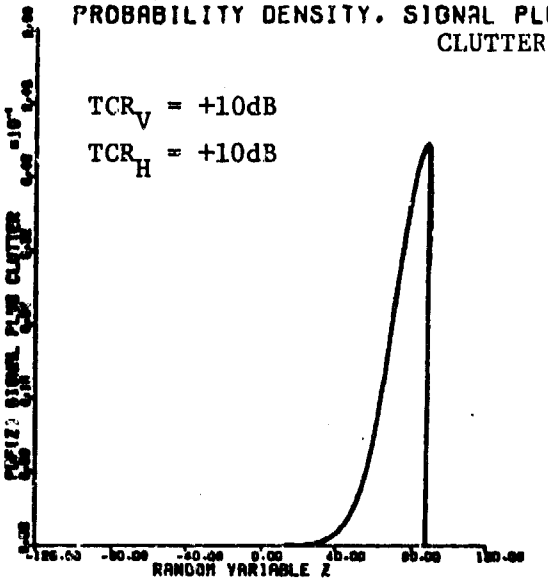

Figure 2.9. Probability density functions of voltage out of the PDC-Phase Only Detector for various target-to-clutter ratios (TCR). Non-uniformly distributed polarimetric phase (shape factor = 1.0) assumed.

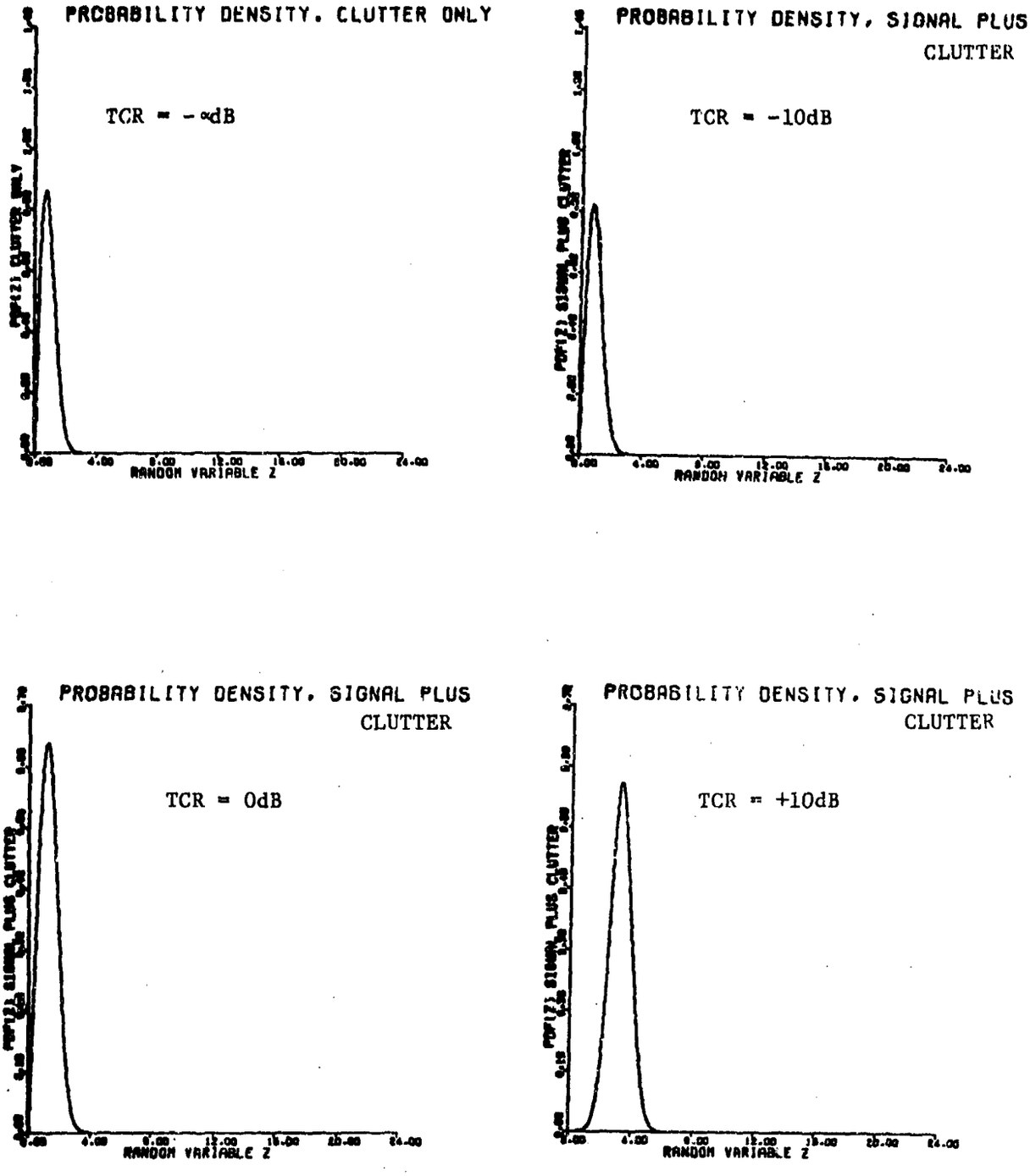

Figure 2.10 Probability density functions of voltage out of square law detector for various target-to-clutter ratios (TCR).

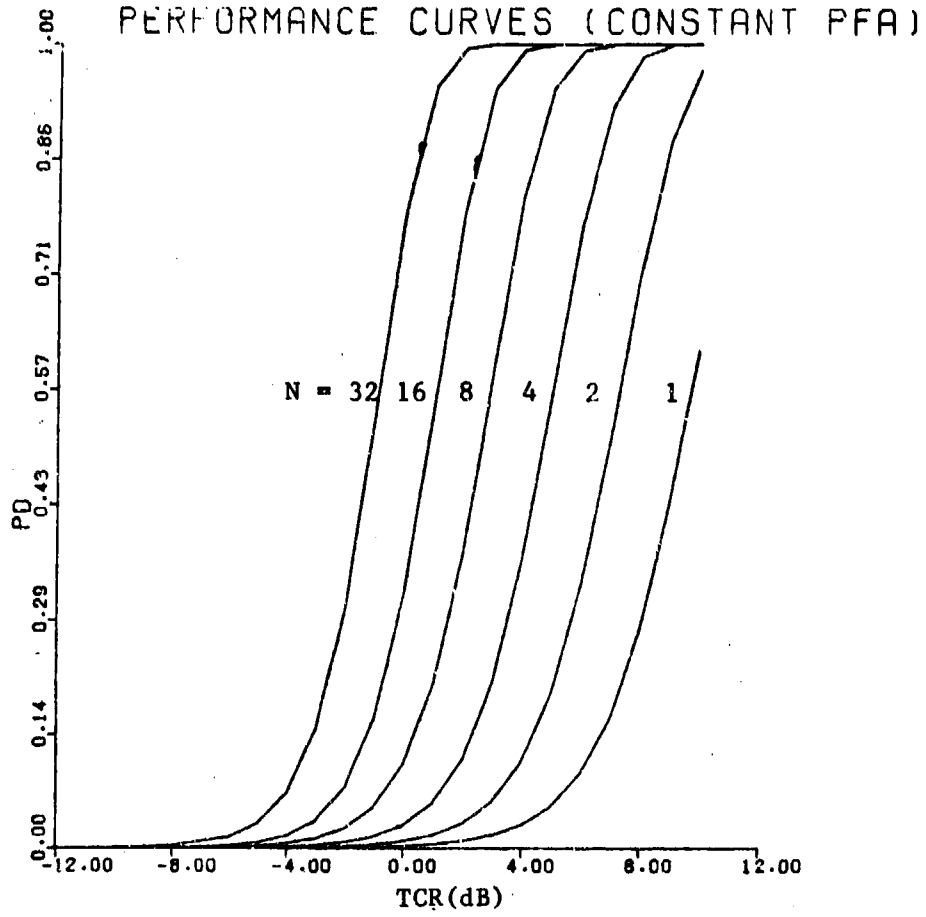

Figure 2.11. Detection performance curves for square law detector (ideal threshold setting). N = number statistically independent pulses integrated, PFA = 10^{-4}.

60 pulses integrated. Please note that while the PCD-dot product and square-law detectors are dependent on an ideally functioning threshold selection processor (a constant false alarm rate device) to provide the performances shown, the PCD-phase only detector does not. Since the latter detector has limiters in it, its clutter density function is not dependent on clutter amplitude levels. Thus, a fixed threshold is adequate to provide the detection performance shown in Figure 2.5

The next section of this report addresses the question of what detection performance can be obtained for the PCD-phase only and square-law detectors when the threshold selection device (CFAR) does not function ideally. Under this type of situation, one might expect the PCD-phase only detector to compare more favorably with the square-law and PCD-dot product detectors.

2.3 INTERCELL PERFORMANCE OF PSEUDO-COHERENT DETECTION

The objective of the foregoing discussion is to provide a basis for evaluating the intercell performance of the pseudo-coherent detection (PCD) technique. In this section of the report, the PCD-phase only technique is compared to a conventional constant-false- alarm rate (CFAR) detection algorithm. Since the PCD-phase only technique has inherent CFAR characteristics, it is desirable to compare it to this type of detection algorithm. The performance of the PCD and amplitude-only CFAR algorithms is determined under both a uniform clutter distribution and a non-uniform clutter distribution. The particular non-uniformly distributed clutter scenario assumed consists of a discontinuity at a particular point in range. On either side of this point in range the clutter is uniformly distributed, but at different levels. The performance of the PCD and CFAR algorithms are evaluated for different target positions relative to this clutter discontinuity. The worst case performance for the amplitude-only CFAR algorithm is when the target is adjacent to the discontinuity.

2.3.1 THEORETICAL AMPLITUDE CFAR DETECTION PERFORMANCE

It is well known that the performance of a fixed threshold detector in the presence of an unknown clutter level is poor. Figure 2.12 illustrates the probability of false alarm as a function of increase in noise power density in dB from design value. As indicated in Figure 2.12 by the dotted lines, if the clutter level is 3 dB larger than that assumed, then instead of obtaining a probability of false alarm of 10^{-8} a probability of false alarm of 10^{-4} will be achieved. This means that the probability of false alarm is

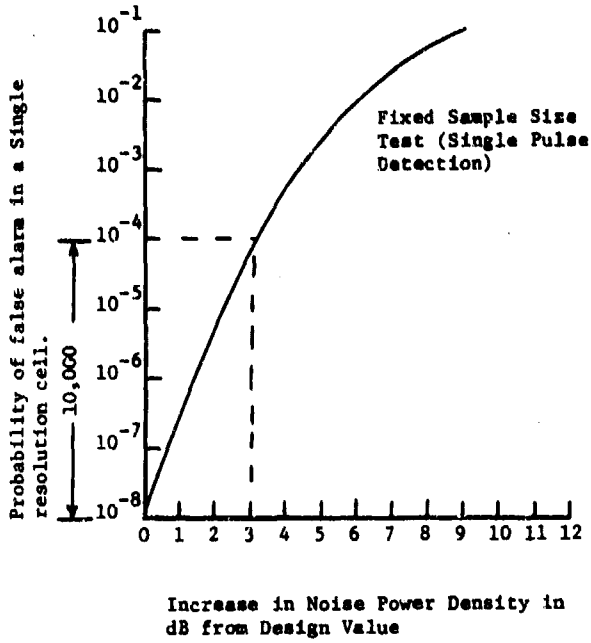

Figure 2.12. Performance of fixed threshold detector in presence of unknown clutter level.

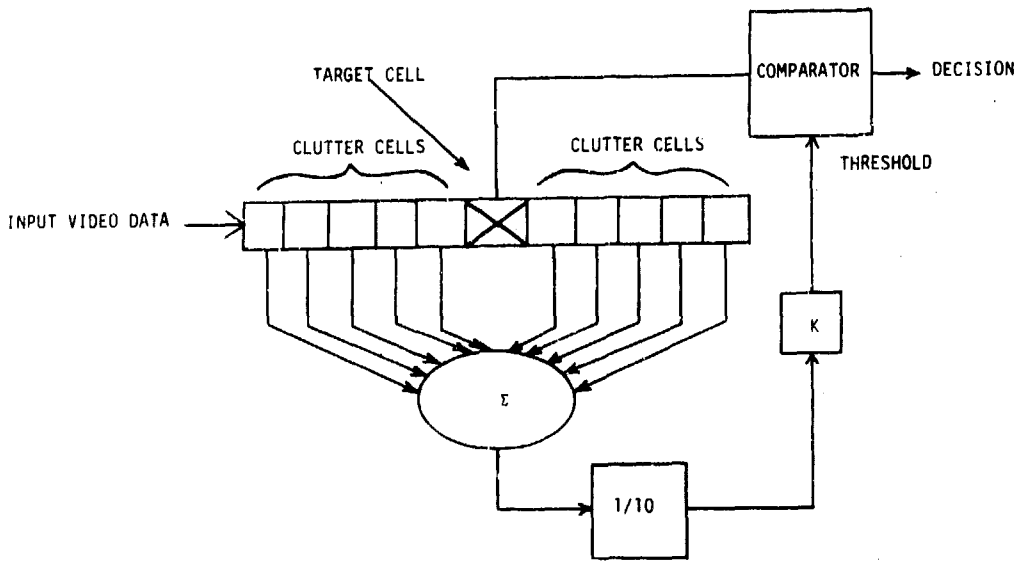

Figure 2.13 Diagram of a 10 cell CFAR device.

increased by 10,000 to 1. Thus the need for a method of estimating the clutter level as accurately as possible. The device used to estimate the clutter level to achieve a constant false alarm rate is called a CFAR algorithm. Typically, a CFAR device averages the clutter found in cells adjacent to the target cell. For example, a CFAR device, as illustrated in Figure 2.13, may consist of 10 range cells, 5 cells on each side of the test cell under consideration. The clutter levels in each of the 10 cells would then be summed and divided by 10 to obtain an estimate of the average clutter level surrounding the test cell. The detection threshold would then be based on this estimated clutter level. In homogeneously spatially distributed clutter, a 10 cell clutter level estimate may still be in error because only 10 samples are used to determine the average clutter level. Thus, a CFAR device with a finite number of range cells does not yield ideal detection performance. Figure 2.14 indicates the detection performance one would obtain with a non-fluctuating target in Rayleigh clutter and where the threshold is set for a probability of false alarm 10^{-4}. For 10 cells (N = 10), one notes that the detection performance is about 2 dB worse than that of the ideal detection curve. In other words, 2 dB more signal-to-noise ratio is required with a 10 cell CFAR than would be required if the clutter level were known. The curve in Figure 2.15 provides the detection loss in dB as a function of the number of resolution cells used in the CFAR device. Note that as the number of cells used decreases, the loss increases. For a 10 cell device with a probability of false alarm 10^{-4} approximately 2 dB is lost because of the error in the CFAR estimate of threshold level.

When the clutter is not homogeneously distributed in range, but consist of a discontinuity as illustrated in Figure 2.16, the performance of the amplitude CFAR algorithm deteriorates noticably. Figures 2.17(a) and (b) indicates how the detection and false alarm proabilities vary with the magnitude of a clutter discontinuity and also with the location of a target relative to the discontinuity for a 40 cell CFAR algorithm[16]. When the target is adjacent to a discontinuity in clutter level, the CFAR device estimates the clutter level to be half way between the two clutter levels. Thus, the threshold is set too high and the probability of detection is lower than desired while at the same time the probability of false alarm is also lower. If the target is a few cells from the clutter discontinuity, the CFAR performs better because fewer of the cells in the CFAR device contain the higher level clutter. Thus the clutter estimate and the threshold setting is closer to that desired. If in the 10 cell example a target is at least 5 range cells from the clutter discontinuity, then only one type of clutter influences the

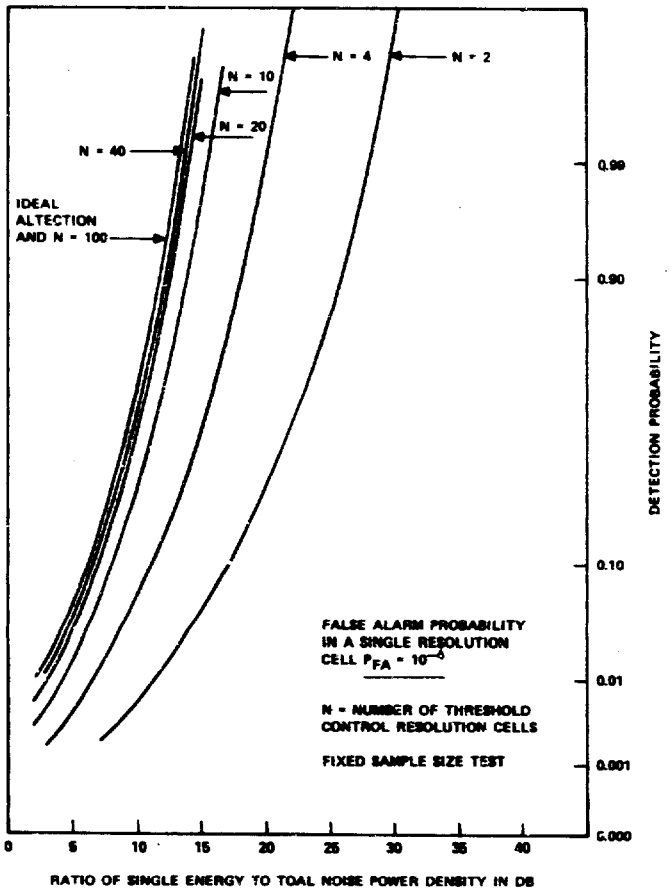

Figure 2.14 Automatic threshold control detection probability for non-fluctuating target, PFA = 10^{-4}.

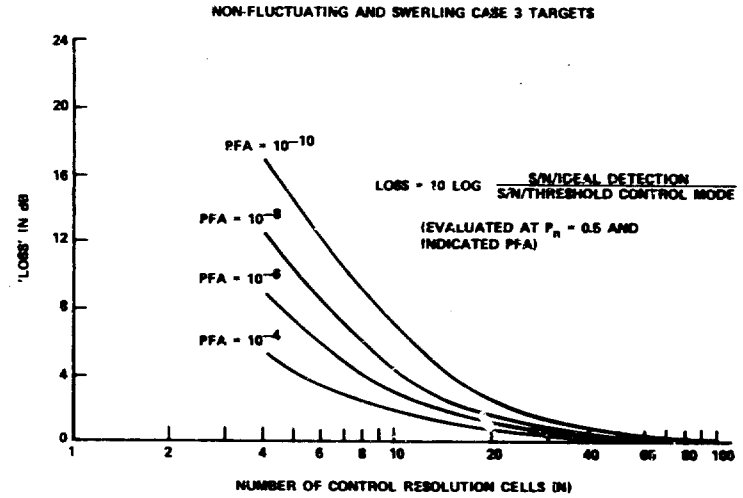

Figure 2.15 Detection loss in dB versus number of threshold control resolution cells, N.

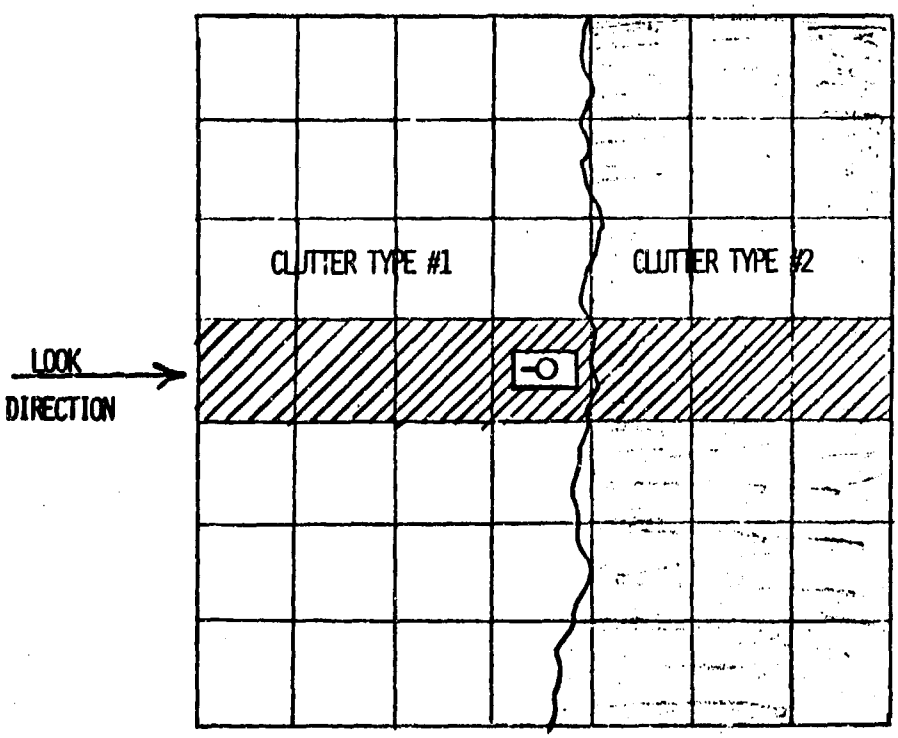

Figure 2.16. Non-uniformly distributed clutter scenario with range-azimuth cells outlined.

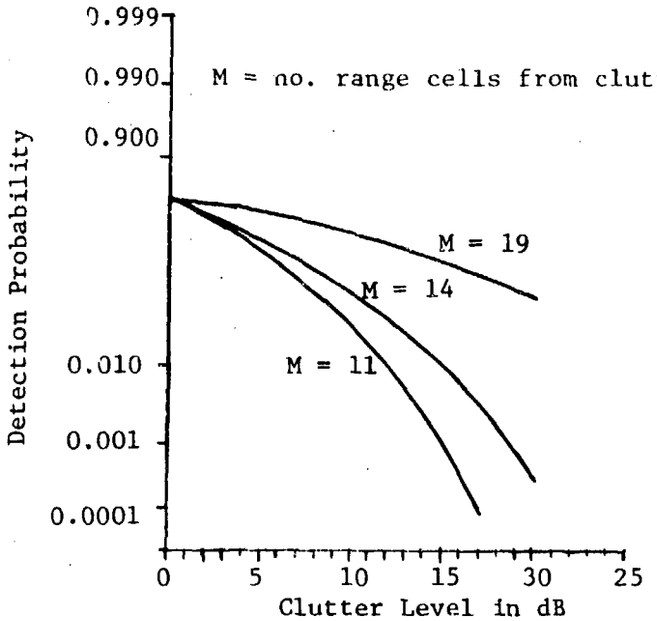

Figure 2.17(a) Probability of detection versus ratio of clutter levels.

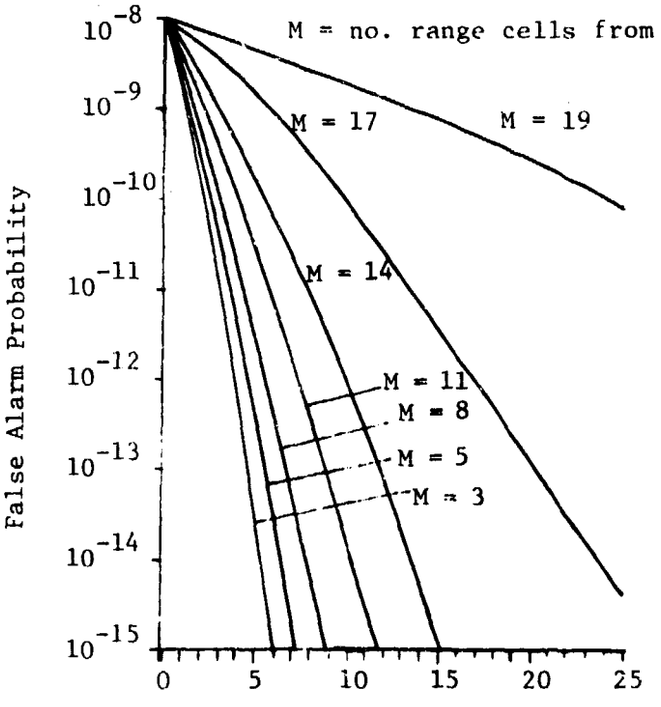

Figure 2.17 (b) False alarm probability versus ratio of clutter levels

CFAR clutter average and threshold setting. Thus, it is only when the target is within 5 cells or less of the clutter discontinuity (in the 10 cell example) that the CFAR device begins to perform poorly. The curves in Figure 2.18 indicate typical detection performance of a 10 cell CFAR device as a function of target position relative to a clutter discontinuity for a fixed ratio of clutter levels. As indicated before, as the target gets closer to the clutter discontinuity the detection and false alarm probabilities decrease. However, if the target is thought to be in the higher clutter, the proper threshold should be based on the higher clutter level, but some of the CFAR cells have the lower clutter in their estimate. Thus, in this case, the threshold is set too low and the probability of false alarm is much higher than that desired. As the target moves away from the clutter discontinuity so that all of the CFAR range cells are filled with the higher level clutter, then the false alarm probability approaches the design value.

In general, the amplitude CFAR detection algorithm will not be able to detect targets in the clear near a clutter discontinuity and the algorithm will falsely detect the leading edge of the higher clutter level. For example, the amplitude CFAR algorithm does not work very well adjacent to a tree line. Other algorithms which overcome this weakness of the CFAR processor are desirable. The PCD-phase only algorithm seems to provide good performance in this type of clutter scenario.

2.3.2 THEORETICAL PSEUDO-COHERENT DETECTION

The theoretical performance of the PCD-phase only detector within a single cell (intracell) has been described and discussed in the previous section of this report. In this section, the theoretical performance of the PCD-phase only algorithm in a multiple cell (intercell) scenario will be addressed. In particular, the performance of PCD as compared to amplitude-only CFAR will be considered. The block diagram of the particular PCD algorithm under consideration in this section is shown in Figure 2.19. The horizontally (H) and vertically (V) polarized received signals are each limited in amplitude and are submitted to a balanced mixer. In effect, the limiters and mixer performs phase detection. However, the phase detected is the relative phase between the H and V receive channels, not the absolute phase of each channel. The mixer output voltage, which is proportional to this relative phase, is subsequently submitted to a threshold and a decision is made relative to a target present or not present. This relative phase shall subsequently be referred to as polarimetric phase.

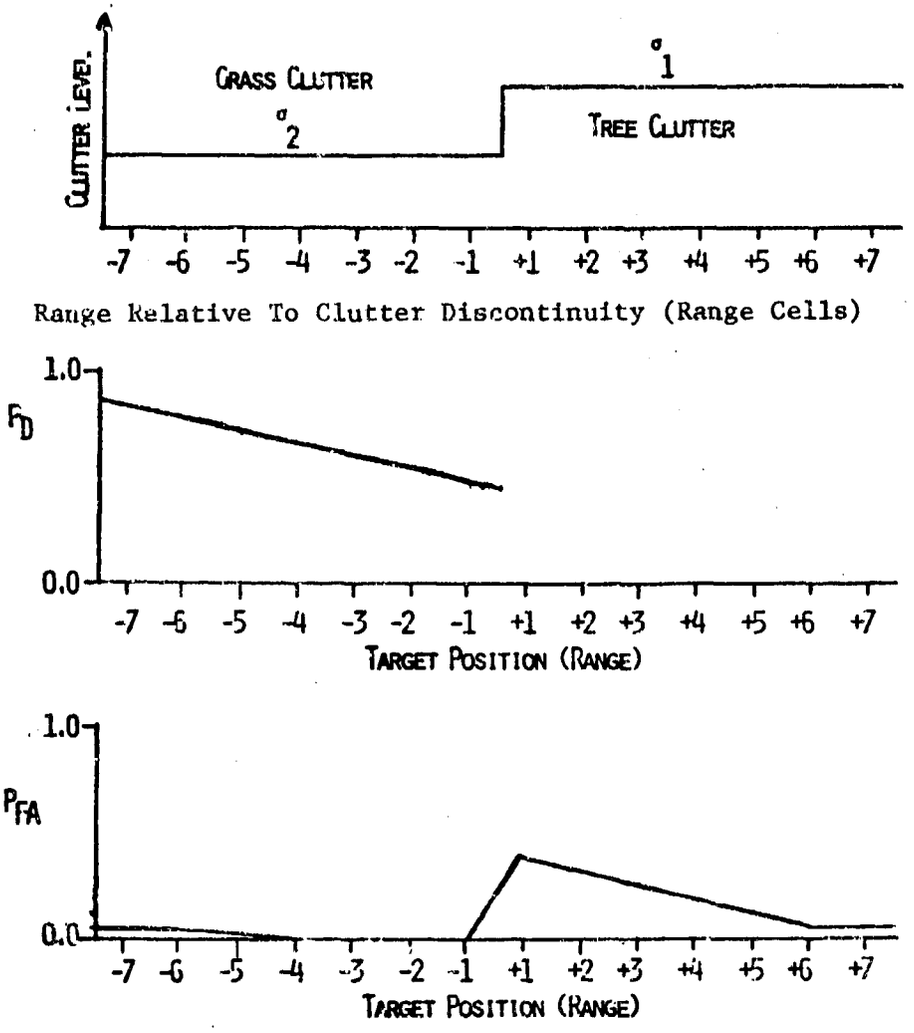

Figure 2.18. Typical detection performance expected with a 10 cell CFAR processor.

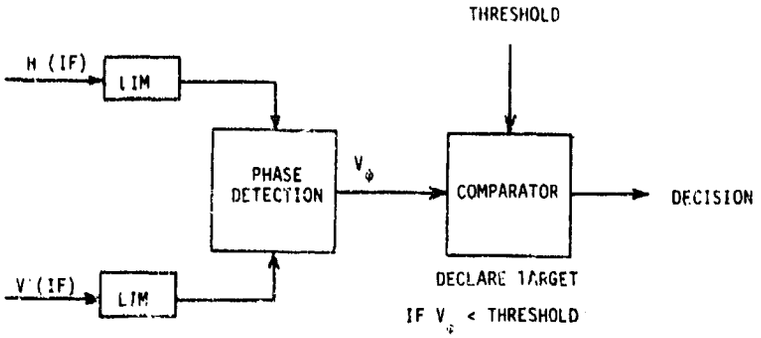

Figure 2.19 Pseudo-coherent detection implementation.

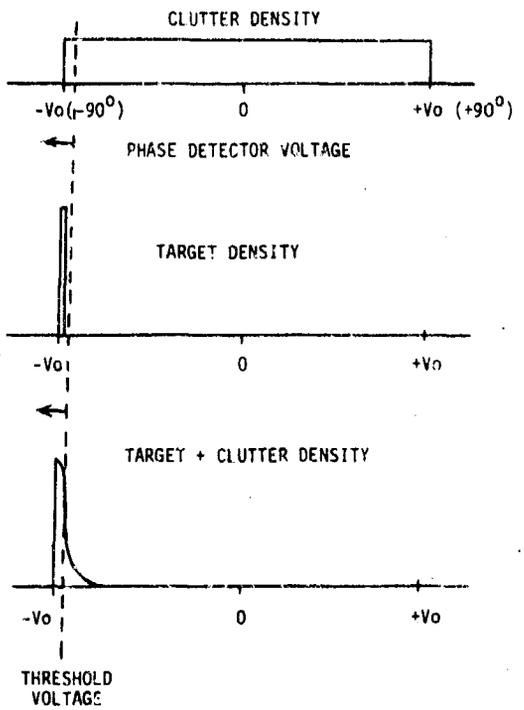

Figure 2.20 Pseudo-coherent detection (PCD) probability density functions (idealized).

In the foregoing discussion, it is assumed that a circularly polarized wave is transmitted. If clutter only is present in the range cell under consideration, and if the clutter consists of many approximately equal-sized scatterers, the polarimetric phase is expected uniformly distributed as illustrated in Figure 2.20. On the other hand, if the object in the cell consists of only one point-source reflector such as a metal plate, corner reflector, or the like, the polarimetric phase will be concentrated near one value of polarimetric phase. The value of phase received will depend on the scatterer type. Odd bounce scatterers (e.g., trihedrals) yield a -90° phase as illustrated in Figure 2.20 while even bounce scatterers (e.g., dihedrals) yield a $+90^{\circ}$ phase value. For the situation illustrated in Figure 2.20, a single threshold is adequate for detecting odd bounce targets. However, since both even bounce and odd bounce targets are expected, a double threshold as illustrated in Figures 2.21 and 2.22 are required.

When non-uniformly spatially distributed clutter, as previously described, is encountered by the PCD-phase only processor, the detection and false alarm performance expected is as shown in Figure 2.23. Since the polarimetric phase threshold is independent of clutter amplitude levels, a change in clutter level does not affect the false alarm probability (P_{FA}). Thus the P_{FA} is the same for each range cell as illustrated in Figure 2.23 and, therefore, the PCD-phase only algorithm provides a constant false alarm rate. However, the target-to-clutter ratio does change with clutter level and, hence, the detection probability does change across the clutter discontinuity as illustrated.

One notes two major advantages of PCD-phase only over amplitude-only CFAR detection: first, there is no false detection of the clutter edge or discontinuity; second, the detection performance in the clear is not affected by the presence of the higher clutter level. Thus a target in a cell adjacent to a tree line could be detected with the PCD-phase only polarimetric processor while it would less likely be detected with an amplitude-only CFAR processor.

2.4 ABERDEEN DATA COLLECTION

Previous research at GIT/EES has shown that various polarimetric processing techniques can provide significant target-to-clutter improvement for those target aspect angles where the horizontally and vertically polarized components of the reflected wave differ in phase by about 90 degrees; however, there is insufficient data available to determine the probability of a 90 degree phase difference for a target aspect angle

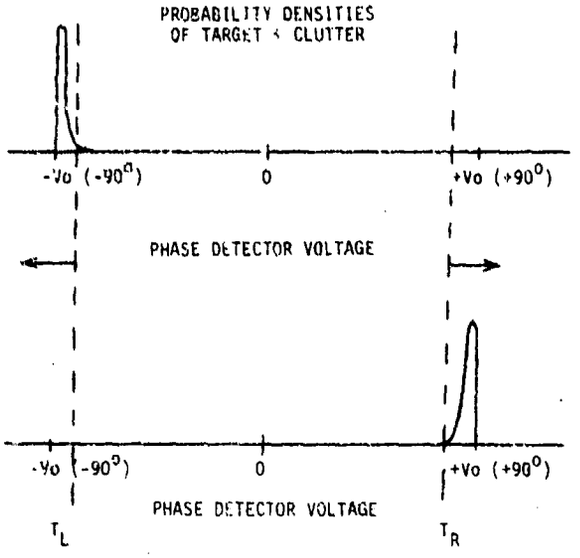

Figure 2.21 Illustration of need for double threshold in pseudo-coherent detection processing.

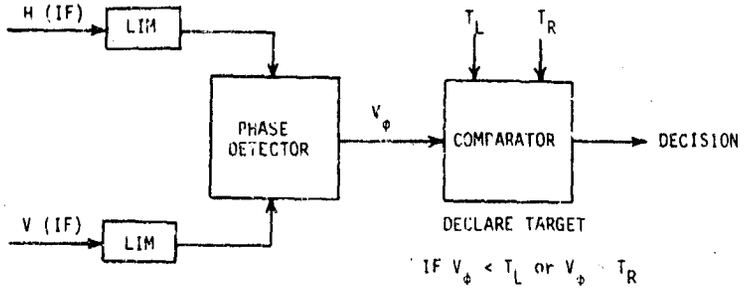

Figure 2.22 Pseudo-coherent detection implementation with double threshold.

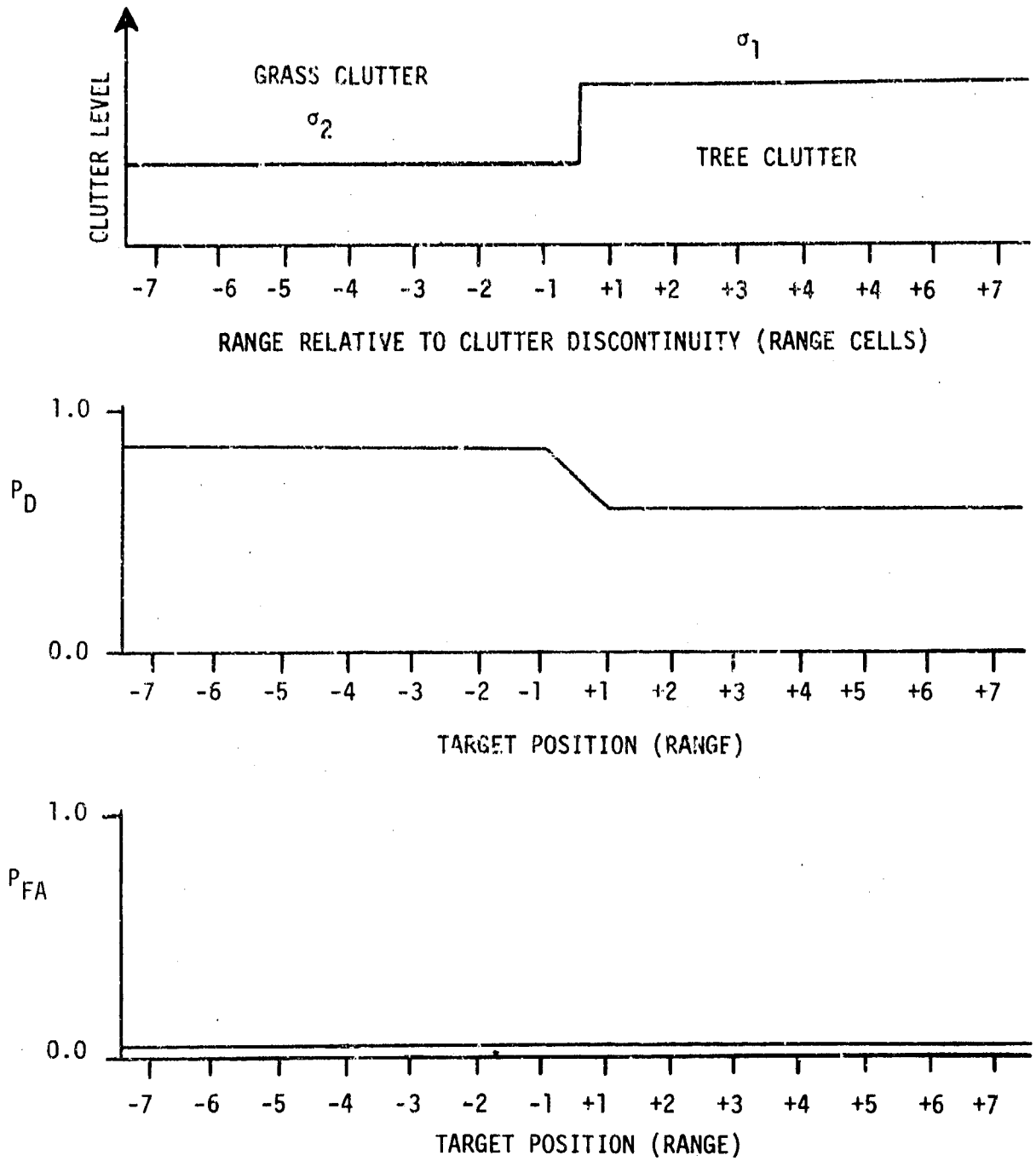

Figure 2.23 Theoretical pseudo-coherent detection performance in a non-uniformly distributed clutter scenario.

selected at random. Therefore, GIT/EES collected experimental data on several tactical targets placed on a turntable using GIT/EES polarization diversity radars. The major purpose of the experiment was to generate data at all aspect angles so that amplitude and polarimetric phase for tactical targets could be characterized statistically. It was proposed that the measurements be conducted at the U. S. Army Aberdeen Proving Ground since targets of interest and a suitable large turntable were available there. A description of the site, the targets used, and the radar configurations employed in the data collection is given in this section.

2.4.1 FIELD SITE

The measurements were made at Field 8, Aberdeen Proving Ground, Maryland. Mr. Jim Andrews was our contact at Aberdeen, and provided personnel and assistance as required for the operation of the target positioner, motor-generator power supply and cranes. In addition, he supplied communications between the equipment tower and the target.

Personnel from ERADCOM, Fort Monmouth, New Jersey erected two closely spaced towers at the field site. A building approximately 6 feet by 12 feet was installed on top of the two towers to house the equipment as shown in Figure 2.24. The building was approximately 8 feet high and contained a 6 foot by 4 foot window, covered with a plexiglas sheet. The window was the only access for loading and unloading large equipment. Personnel and small equipment entered through a "trap door" located in the floor of the building. Steps were provided from the ground to the building floor. The tower was 70 feet high and was located approximately 700 feet from the target positioner. A view of the target positioner from the tower is shown in Figure 2.25 and a close-up view of a tank on the target positioner is shown in Figure 2.26. All radar and data recording equipment was located on the tower. Data reduction equipment was located in a van at the tower base for "quick look" data analysis.

The target positioner was a large, wood covered turntable capable of supporting very heavy targets. The minimum rotational speed of the positioner, to maintain constant velocity (prevent jerking motion), is 1 degree per second or 6 minutes per revolution. Georgia Tech installed an incremental encoder and a micro-switch on the positioner to provide an angular position readout. The encoder was driven by a 1:1 timing gear from the main drive sprocket. Output from the encoder was a series of 2,000 pulses per encoder revolution or greater than 10,000 pulses per target revolution. The micro-

Figure 2.24 Photograph of towers and building which housed the radar measurement equipment.

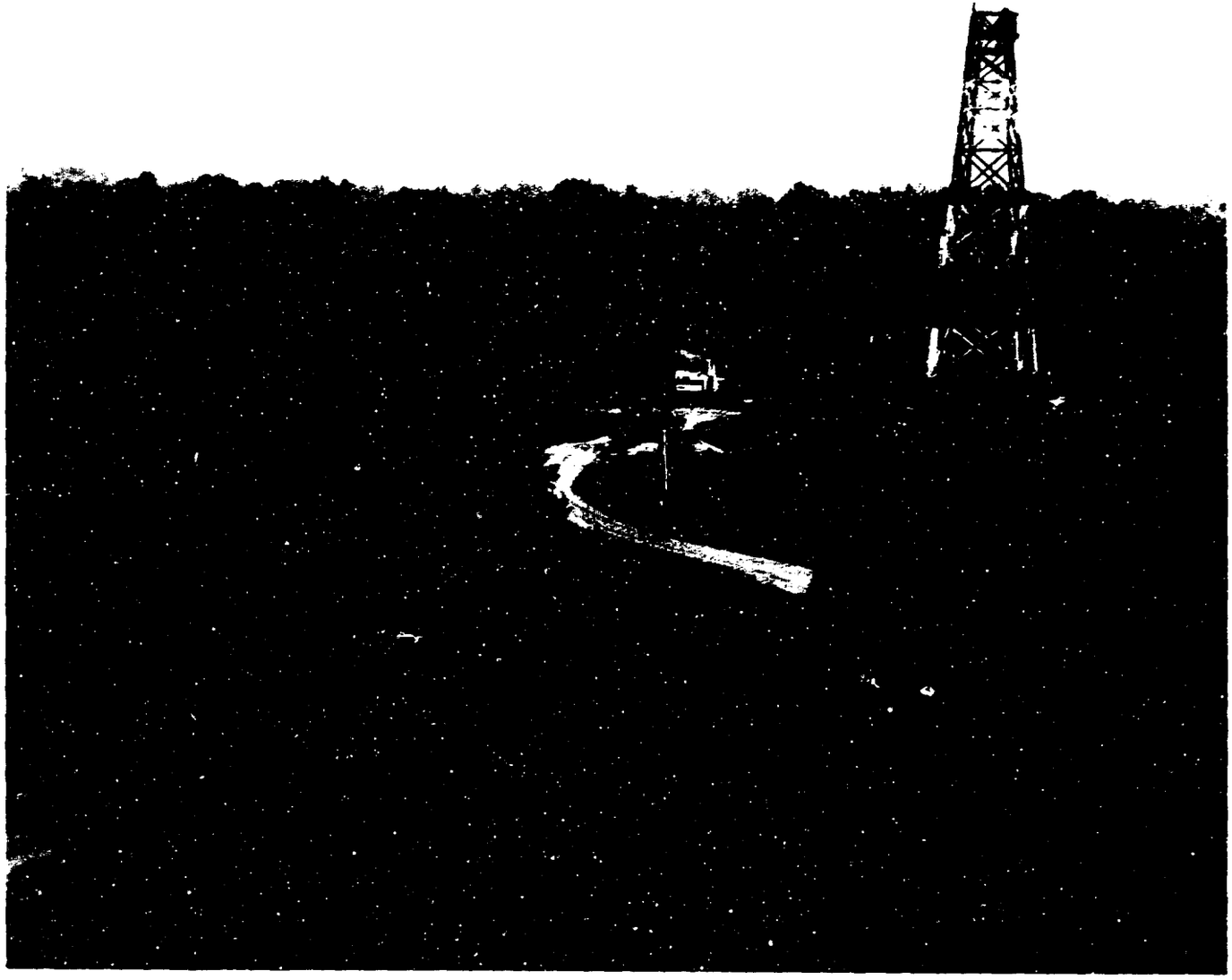

Figure 2.25 A view of target positioner from the radar measurement tower.

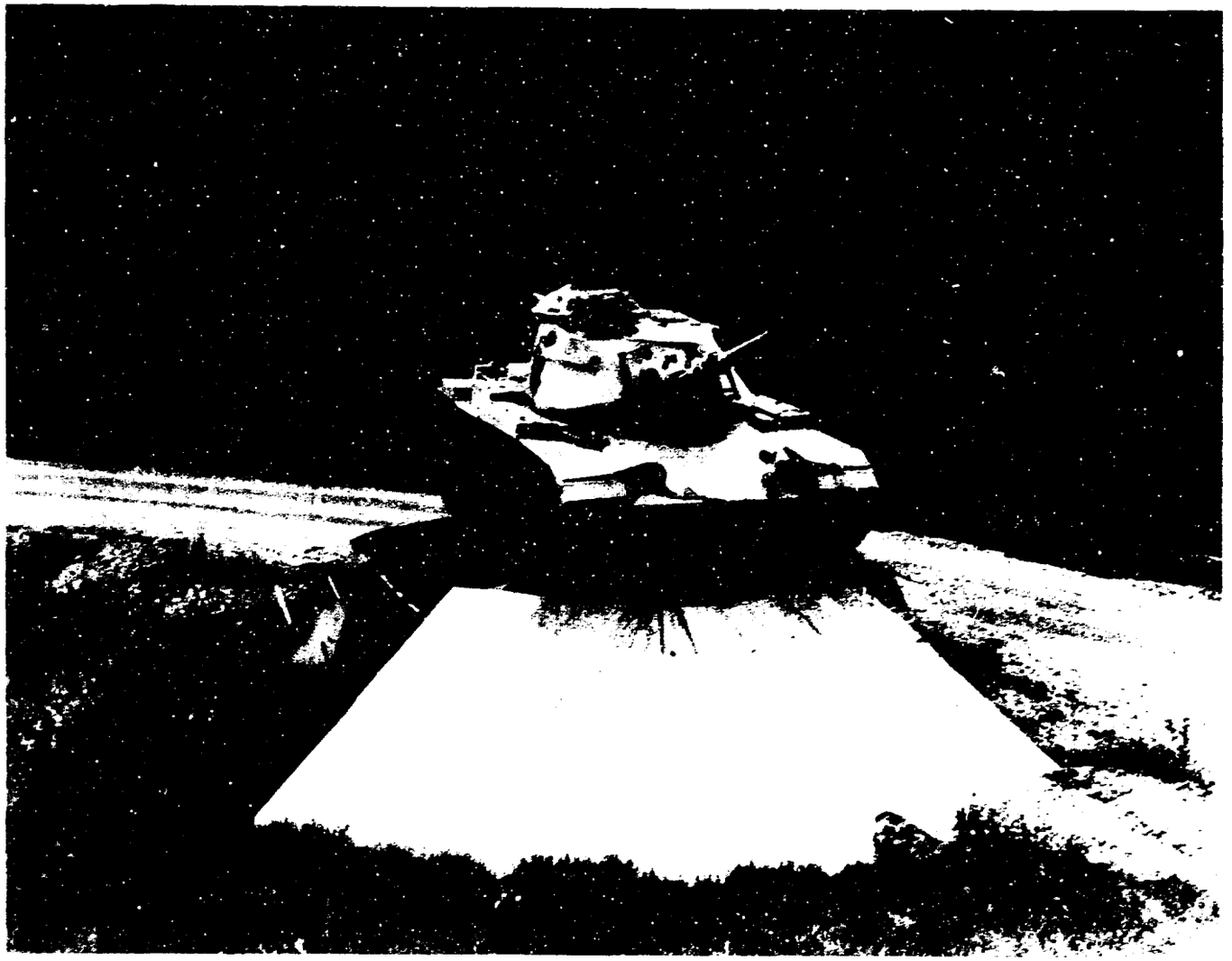

Figure 2.26 Close-up view of a tank on the target positioner. The plywood skirt to reduce radar reflections from positioner is shown in the foreground.

switch closed once each target revolution. These two signals were processed and recorded on the data tape. A skirt of wood was used to mask the effects of the rotating components of the positioner and to reduce the magnitude of the radar return from the positioner. A view of the positioner and skirt is shown in Figure 2.26.

There are two towers near the location of the target positioner and there was an interference problem associated with the tower nearest the positioner using the 150 nanosecond pulse. Therefore, it was necessary to reduce the transmitted pulse length to 75 nanoseconds in order to eliminate this source of interference. Also, trees located in the vicinity of the measurement site were removed to further reduce interference.

Calculations based on the known geometry of the measurement site indicated that the effect of multipath would not be a serious problem. Spacing between nulls generated by the interference of direct and indirect rays at 9.4 GHz are in the order of 15 cm. This close spacing compounds the problem of verifying that multipath effects are not present since a target (corner reflector) which is physically small compared to 15 cm is required. Such a small target is difficult to detect in the presence of the target support and ground clutter. However, an attempt was made to define as well as possible the characteristics of the illuminating electromagnetic field in the vicinity of the target using both large and small targets (corner reflectors).

2.4.2 RADAR SYSTEMS

Measurements were made at both X-band and 94 GHz frequencies. Several transmit/receive modes were used and the data were recorded on a FM magnetic tape recorder. The radar data were in the form of stretched (box-carred)samples of single cell amplitude and polarimetric phase signals from the targets of interest. Target aspect angle data was simultaneously recorded with the radar data.

2.4.3 X-BAND RADAR

Three configurations of the X-band radar were necessary to collect the required data, however, the transmitter for all three system configurations was not changed. The transmitter is a master oscillator-power amplifier (MOPA) chain using a 50 mW varactor tuned Gunn oscillator as the basic source. The X-band signal generated in the Gunn source is pulse modulated through two series connected Watkins Johnson M14A balanced mixers. The modulated signal from the two balanced mixers may be varied from a continuous CW signal to pulses as short as 15 ns. This signal is amplified in the first TWT

to a level of 1 watt. A second pulse modulated TWT amplifier then amplifies the signal to the final value of 1 kW. The Gunn source may be operated in a fixed frequency mode or its frequency may be changed on a pulse-to-pulse basis over a frequency range of $\pm$150 MHz.

Transmit modes were determined by the arrangement of the waveguide between the transmitter and the antenna. Receive modes were determined by the point at which the received signal is coupled from the waveguide into the receiver assembly. The receiver assembly is common to all three transmitter configurations and is shown in Figure 2.27. The simplest radar configuration is shown in Figure 2.28. Using this waveguide arrangement the system is capable of transmitting signals with fixed horizontal, fixed vertical or alternating (on a pulse-to-pulse basis) between horizontal and vertical polarizations. The signals received in the two receiver channels are either parallel to (P channel) or orthogonal to (C channel) the transmitted polarization.

The second X-band radar configuration is shown in Figure 2.29. This system is similar to the one shown in Figure 2.28 except that a four port 90 degree hybrid, a phase shifter and a compensating attenuator has been added. Power entering either input port of the 90 degree hybrid is equally divided between the two output ports. One output port will either lead or lag the others by 90 degrees depending on which input port is activated by the switchable circulator. The two signals are fed to the orthogonal ports of a dual mode coupler, resulting in a transmitted signal which may be adjusted from a pure linear polarization in a plane 45 degree to the orientation of the dual mode coupler to a pure circular polarization. Linear polarization results when the two signals are in phase at the dual mode coupler and circular polarization results when the two signals are separated by 90 degrees. The receiver in this configuration is connected to the waveguide so that the parallel and cross channels represent the components of the reflected wave which are either parallel to or orthogonal, respectively, to the polarization of the transmitted wave.

The third configuration for the X-band radar is shown in Figure 2.30. In this sytem the waveguide is connected the same as previously except that circulators have been inserted at the antenna ports. This allows the same polarization modes to be transmitted but the receiver is capable of receiving only the horizontal and vertical components of the reflected radar signal.

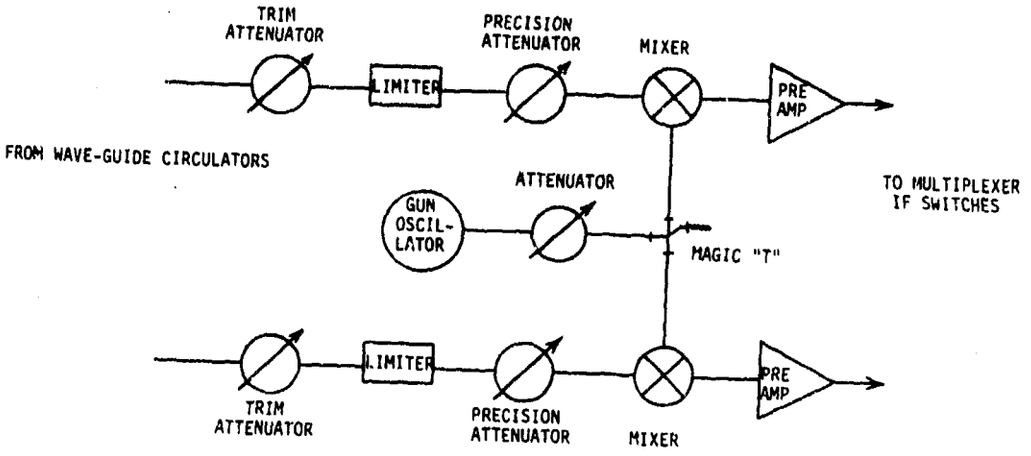

Figure 2.27 X-band radar receiver assembly.

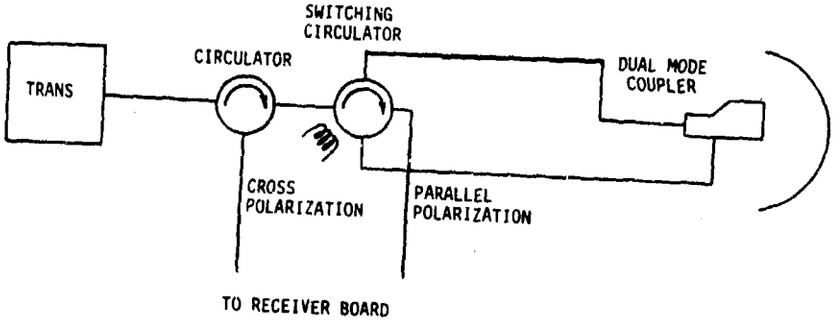

Transmit Modes

1. Fixed Horizontal
2. Fixed Vertical
3. Alternate H, V

Receive Modes

1. Fixed Horizontal
2. Fixed Vertical
3. Alternate H, V

Figure 2.28 X-band radar configuration one.

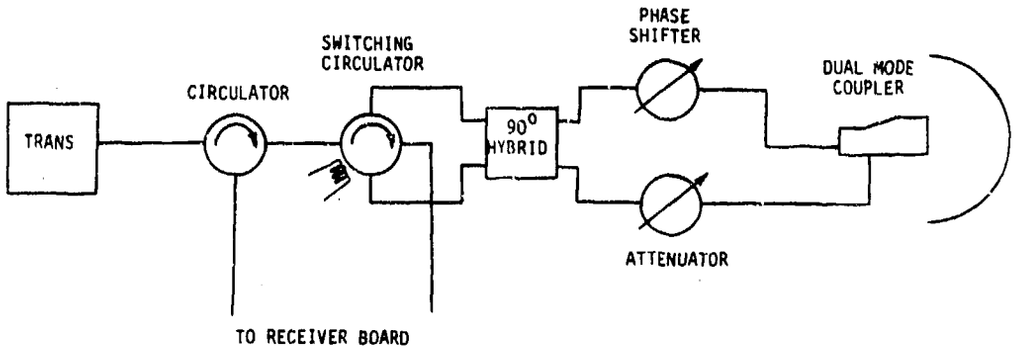

Transmit Modes

1. Fixed R/L Circular
2. Alternate R/L Circular
3. Alternate 45 Degree Linear
4. Fixed 45 Degree Linear

Receive Modes

1. Fixed R/L Circular
2. Alternate R/L Circular
3. Alternate 45 Degree Linear
4. Fixed 45 Degree Linear

Figure 2.29 X-band radar configuration two.

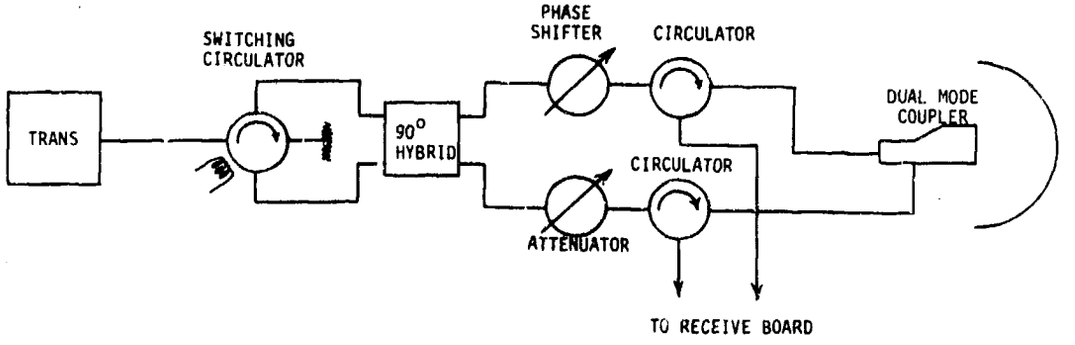

Transmit Modes

1. Fixed R/L Circular
2. Alternate R/L Circular
3. Fixed 45 Degree Linear
4. Alternate 45 Degree Linear

Receive Modes

1. Fixed Horizontal and Vertical

Figure 2.30 X-band radar configuration three.

2.4.4 95 GHz RADAR

A complete block diagram of the 95 GHz radar is shown in Figure 2.31. The system is capable of transmitting either fixed or alternating vertical, horizontal, or 45 degree linearly polarized signals as well as fixed or alternating right and left circularly polarized signals. The receiver is connected so that only the horizontal and vertical components of the reflected radar signal are detected.

2.4.5 CALIBRATION AND PROCEDURES

Calibration of the radar return was achieved by placing a corner reflector of known radar cross section in front of the target and recording the amplitude of the video signal from this range cell. The RF attenuator in the radar receiver was stepped in 5 dB decrements over the dynamic range of the signal. Using this technique, the calibration levels were in units of radar cross section and only a range correction was required. This is a reliable method of calibration provided the electromagnetic field at the target is not contaminated with multipath or reflections from other objects located in the same resolution cell. To insure that the field is uniform at the calibration target's location, a vertical field probe was used to determine if multipath effects were present.

A separate calibration or reference signal is required for each radar mode. Each day a step calibration was made to generate a receiver transfer characteristic prior to the first target run. This step calibration was made with a diplane oriented 22.5 degrees from vertical and using both vertical and horizontal polarizations. After the receiver transfer characteristic was recorded each data run was preceded by a 10 second sample of the radar return from an appropriate target or targets of known radar cross section. For this 10 second sample, the radars were operated in the applicable polarization/frequency/resolution modes.

2.4.6 DATA COLLECTION PROCEDURES AND TEST MATRIX

Data were collected for the various radar modes shown in the test matrix for five military targets as well as trees and grass. Targets which were placed on the turntable were rotated in azimuth through 720 degrees. Each target was placed on the turntable so that it was facing away from the radar near the zero degree position of the turntable. A description of four of the five targets used in this data collection is given in Tables 2.1 through 2.4. No information was available on the 2 1/2 ton truck used in the data collection. The combinations of frequency mode, transmit polarization mode, receive

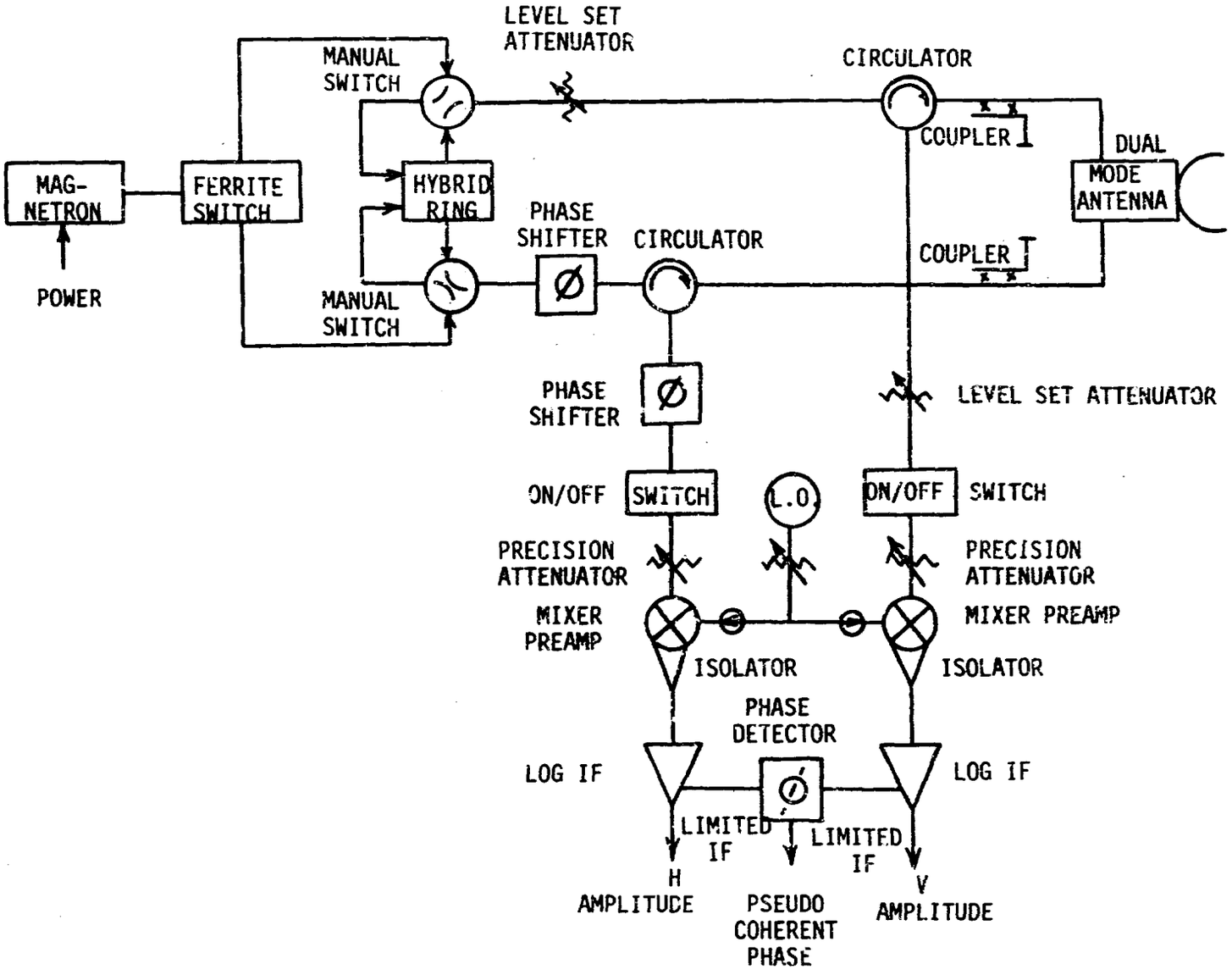

Figure 2.31 95 GHz radar transmitter-receiver block diagram.

TABLE 2-1. DESCRIPTION OF HOWITZER, LIGHT, SELF-PROPELLED, 105MM, M108

Weight Classification	Cross Country Loaded Class 20
Weight	46, 921 pounds
Length	240- 1/2 inches
Width	124 inches
Height	120 inches
Fuel	137 gallons
Range	220 miles
Speed	35 miles per hour

TABLE 2.2. DESCRIPTION OF TANK, COMBAT, FULL TRACKED, 105 MM GUN, M60 AND M60A1

	M60	M60A1
Weight Classification	Cross Country Loaded - Class 50	
Weight (empty)	95,300 pounds	97,494 pounds
Length	320 inches	325 inches
Width	144 inches	128.20 inches
Fuel	385 gallons (Diesel)	375 gallons (Diesel)
Engine (continental):		
Cylinders	12	12
Model Number	AVDS 1790-2	AVDS-1790-2A
Type (both models)	90^{o}, V-Type, Air-Cooled, Diesel	
Transmission, GMC (Allison Division):		
Model	CD 850-6	CD-850-6A
Type	Cross Drive	Single Stage

Differences Among Models:

The turrets are of different design. Also, the external storage rack of the M60A1 extends completely around the rear of the turret and the lower portion is screened.

TABLE 2.3. HOWITZER, LIGHT, TOWED, 105MM, M102

Classification ..... Standard A
Weight Classification ..... Empty - Class 2

Components:

Cannon	Carriage	Recoil Mechanism
M137MOD	M31	M37

Length:

Travel Position ..... 262 - 1/2 inch
Width ..... 76 inches
Weight ..... 3,140 pounds

Cannon:

Weight ..... 900 pounds
Length ..... 131 inches
Type of Breechblock ..... Vertical Sliding Wedge Manual
Type of Firing Mechanism ..... Inertia Percussion, Mechanical
Muzzle Velocity ..... 2,225 FPS
Rate of Fire ..... Max SPM - 10, Sustained SPM - 3
Estimated Accuracy Life of Tube ..... 3,000 RD

Carriage:

Height ..... 47 inches
Length ..... 176 inches

Recoil Mechanism:

Type M37
Length of Recoil ..... Variable, from 30 to 50 inches
Equilibrator ..... Springs

TABLE 2.4. TRUCK, UTILITY, 1/4-TON, 4 x 4, M151, M151A1, M151A2.

Classification	Standard B
M151, M151A1	Standard A
Engine (Ford, Army Design, 4 cyclinders)	2805-678-1820
Transmission (Selective Synchromesh)	2520-678-1808
Weight:	
M151	2,273 pounds
M151A1, M151A2	3,600 pounds
Length	132.7 inches
Width	64 inches
Height	85 inches
Tires	7.00 x 16
Battery	2 (12 V) 24 V System
Fuel	17 gallons
Range	300 miles
Speed	65 miles per hour

Differences Among Models:

The M151A1 has an improved suspension system over the M151. The M151A2 has a more improved front and rear suspension, two-speed electrical wipers, manually operated washers, a one-piece windshield, a mechanical fuel pump, and integrated exterior lighting at front and rear of vehicle.

polarization mode, radar tranamit frequency and range resolution utilized in this measurement program are indicated in the Test Matrix in Table 2.5.

TABLE 2.5. TEST MATRIX - VEHICLE TARGETS

Frequency Mode	Transmit Polarization Mode	Receive Polarization Mode	Radar Frequency Bands	Range Resolution (NS)	X-Band Radar Configuration
Fixed	Fixed Circular	H, V, sin ϕ	X & 95	75	Figure 2.30
Fixed	Agile Circular	H, V, sin ϕ	X & 95	75	Figure 2.30
Agile	Fixed Circular	H, V, sin ϕ	X	75	Figure 2.30
Agile	Agile Circular	H, V, sin ϕ	X	75	Figure 2.30
Agile	Fixed 45^0	H, V, sin ϕ	X	75	Figure 2.30
Agile	Agile 45^0	H, V, sin ϕ	X	75	Figure 2.30
Fixed	Fixed Circular	H, V, sin ϕ	X & 95	20	Figure 2.30, *Range Profile
Agile	Alternate H-V	P, C, sin ϕ	X	75	Figure 2.28
Agile	Fix H	P, C, sin ϕ	X	75	Figure 2.28
Agile	Agile Circular	P, C, sin ϕ	X	75	Figure 2.29
		CLUTTER TARGETS			
Fixed	Fixed Circular	H, V, sin ϕ	X & 95	75	Figure 2.29
Fixed	Alternate H-V	P, C, sin ϕ	X & 95	75	Figure 2.28
Agile	Fixed Circular	H, V, sin ϕ	X	75	Figure 2.30

SECTION 3
SUMMARY

Results of a study to determine the performance of one particular class of discrimination algorithms utilizing polarimetric phase have been presented. Since one of these processors, the PCD-phase only processor, is a single range cell constant false alarm process, a distinction between its performance in a single cell and in a multiple range cell scenario has also been made. In a theoretical comparison of the PCD-dot product, PCD-phase only, and square-law detection (SLD) processors, it was assumed that ideal threshold settings were available for the PCD-dot product and square law detectors. However, such an assumption was not necessary for the PCD-phase only detector. Under this assumed situation, the PCD-dot product detector requires from 1.6 to 3 dB less target-to clutter ratio (TCR) for the same PD and PFA than the square-law detector. The 3 dB advantage exists for single pulse detection while the 1.6 dB improvement is for a very large number of pulse integrations. Also under the above assumption, the PCD-phase only and square-law detectors have approximately equivalent detection performance for an integration of 60 pulses or more. However, the PCD-phase only detector performance is not as good for less than 60 pulses integrated.

However, when the effect of adding a CFAR device to a conventional square-law detector (SLD) is taken into account, the PCD-phase only processor has better performance than the SLD/CFAR in some clutter scenarios. Specifically, one notes two major advantages of PCD-phase only over SLD/CFAR detection: first, there is no false detection of a clutter edge or discontinuity; second, the detection performance in the clear is not affected by the presence of the higher clutter level. Thus a target in a cell adjacent to a tree line could be detected with the PCD-phase only polarimetric processor while it would less likely be detected with an SLD/CFAR processor.

X-band and 94 GHz radar data were collected on five military tarets over 720 degrees of aspect angle. This data was collected to support computer simulation of polarimetric processors utilizing measured data. Each target was placed on a turntable and radar data was taken as the target rotated. In addition, data was taken on nearby grass and tree clutter. Combinations of frequency modes, transmit polarization modes, receive polarization modes, radar transmit frequencies (9.4 and 94 GHz), and range resolutions were utilized. The interpretation and processing of this data will be performed under a later contract.

THIS PAGE IS INTENTIONALLY LEFT BLANK

APPENDIX A
MATHEMATICAL MODEL OF TWO DISCRIMINATION PROCESSORS

The mathematical model of a two channel radar receiver is shown in Figure A-1. The transmitted signal is assumed to be

$$S_T(t) = A\cos\left[\omega_o t + \theta(t)\right] ; nT \leq t \leq n(T+\tau) \tag{A-1}$$

where

T	is the interpulse period
τ	is the pulse length
n	is the nth pulse transmitted
A	is the amplitude (voltage)
ω_o	is the transmitted frequency
$\theta(t)$	is the unknown phase associated with a non-coherent source

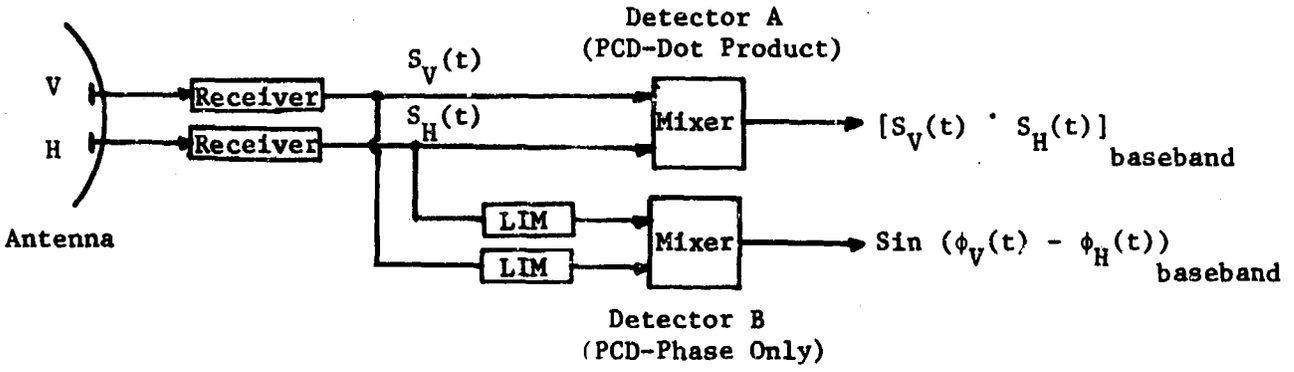

Figure A-1. Model of radar receiver and detection circuitry.

The received signal is assumed to be a large sum of attenuated and time delayed transmitted signals, all from the same range cell. This assumption is valid when clutter is present and consists of a large number of scatterers in one range cell. Thus, the received signal is given by

$$S_R(t) = \sum_{i=1}^{N} K_i A \cos\left[\omega_o t + \theta(t) + \phi_i\right] \tag{A-2}$$

where

Ki is the attenuation factor (a function of range, reflection coefficient, etc.)

N is the number of scatterers in one range cell, and

ϕ_i is the phase shift introduced by each scatterer and is assumed to be randomly distributed over 0 to 2 π radians.

The received signal given by Equation (A-2) may be considered as having in-phase and quadrature components as follows:

$$S_R(t) = \sum_{i=1}^{N} (K_i A \cos\phi_i) \cos\left[\omega_o t + \theta(t)\right] - \sum_{i=1}^{N} (K_i A \sin\phi_i) \sin\left[\omega_o t + \theta(t)\right] \tag{A-3}$$

or as

$$S_R(t) = X(t)\cos\left[\omega_o t + \theta(t)\right] - Y(t)\sin\left[\omega_o t + \theta(t)\right] \tag{A-4}$$

where

$$Y(t) = \sum_{i=1}^{N} K_i A \sin\theta_i \tag{A-5}$$

$$X(t) = \sum_{i=1}^{N} K_i A \cos\phi_i \qquad \text{(A-6)}$$

X(t) and Y(t) may be considered as random processes for both clutter only and clutter plus target.

For the clutter only case, X(t), Y(t) are each assumed to be Gaussian distributed with zero mean and with variance (σ^2) equal to clutter power (P_c). They are also assumed to be statistically independent. These assumptions are valid if the range cell under consideration contains a large number of approximately equal-sized scatterers.

When a target (non-fluctuating) is present with clutter in the range cell, the combined target plus clutter signals, X(t), Y(t), may be modeled as Gaussian with non-zero means, a and b, respectively. Since the amplitude and phase modulation are related to X(t) and Y(t) as

$$A(t) = \sqrt{X^2(t)+Y^2(t)} \qquad \text{(A-7)}$$

$$\phi(t) = \tan^{-1}\left[\frac{Y(t)}{X(t)}\right] \qquad \text{(A-8)}$$

the in-phase and quadrature means, a and b, are related to the means of A(t) and ϕ (t) as follows:

$$\overline{A(t)} = \sqrt{a^2 + b^2} \qquad \text{(A-9)}$$

$$\overline{\phi(t)} = \tan^{-1}\left(\frac{b}{a}\right) \qquad \text{(A-10)}$$

Thus, specification of a and b not only defines the mean of the amplitude modulation, but also defines the mean of the phase modulation.

The received signal given by Equation (A-4) may represent the signal in either the horizontal polarization channel or the vertical polarization channel. Thus, the signals in these two channels may be written as

$$S_V(t) = X_V(t)\cos\left[\omega_o t + \theta(t)\right] - Y_V(t)\sin\left[\omega_o t + \theta(t)\right] \tag{A-11}$$

and

$$S_H(t) = X_H(t)\cos\left[\omega_o t + \theta(t)\right] - Y_H(t)\sin\left[\omega_o t + \theta(t)\right] \tag{A-12}$$

In Figure A-1, two types of detectors are presented. Detector A utilizes all the information in each receive channel-both amplitude and phase modulation information. This detector is called the Dot-Product detector since it forms the product of the signals in the two receive channels. Detector B in Figure A-1 has amplitude limiters in each receive channel preceding the mixer. Thus, the output of the mixer provides only the cosine of the phase difference. Note that the unknown transmitted phase, $\theta(t)$, does not appear at the detector's output. Thus, the radar does not have to be coherent when used with either of these two detectors.

In the subsequent text, mathematical equations will be derived to represent the probability density functions at the output of both detectors. As will be shown, several different clutter models will be assumed. The justification for each model will be given.

DETECTOR A (PCD - DOT PRODUCT)

The output of the mixer in detector A involves the amplitude of the signal in each channel as well as the relative phase between channels, $(\phi_V - \phi_H)$. Thus, the mixer output is given by

$$O(t) = \left[S_V(t) \cdot S_H(t)\right]_{\text{baseband}} \tag{A-13}$$

where $S_V(t)$ and $S_H(t)$ are defined by Equations (A-11) and (A-12). Substituting these equations into (A-13) and simplifying, one obtains

$$O(t)=X_V(t) \cdot X_H(t)+Y_V(t) \cdot Y_H(t) \tag{A-14}$$

As indicated earlier, X(t) and Y(t) can be assumed to be Gaussian distributed with mean and variance related to the target and clutter levels. To obtain the probability density function for the mixer output, O(t), the following two probability relationships are used. First, the product of two Gaussian random variables, $Z = X \cdot Y$, is given by[17]

$$f_Z(Z)=\int_{-\infty}^{\infty} \frac{1}{|\omega|} f_{XY}(\omega,\frac{Z}{\omega}) \, d\omega \tag{A-15}$$

where $f_{XY}(.,.)$ is the joint density function of the random variables X and Y. Second, the probability density function of a sum of two random variables, $Z = X + Y$, is

$$f_Z(Z)=\int_{-\infty}^{\infty} f_{XY}(Z-Y,Y)\,dY \tag{A-16}$$

where $f_{XY}(.,.)$ is as previously defined. The derivation of the density function for O(t) in Equation A-14 is given in Reference 18 for a non-zero mean case. The expression for the density function of O(t) is extremely complicated and difficult to work with. However, its Fourier transform, called the Characteristic equation, is also derived and is a much simplier expression. Thus, as described in Section 2, the Characteristic equation for O(t) was utilized and is given by[18]

$$C(\omega)=\frac{\mathrm{Exp}\left[(j\omega\rho)/(1+\omega^2/4)\right] \cdot \mathrm{Exp}\left[(-\rho^2\omega^2)/(1+\omega^2/4)\right]}{(1+\omega^2/4)} \tag{A-17}$$

where ρ is the voltage signal-to-noise ratio, $A/\sqrt{2}\sigma_c$ and ω is the Characteristic equation variable (not frequency).

DETECTOR B (PCD - PHASE-ONLY)

The output of the mixer for this case will only involve the phase of the H and V receive signals since the mixer is preceded by limiters. Thus, the mixer output is given by

$$O(t) = \sin\left[\phi_V(t) - \phi_H(t)\right] \tag{A-18}$$

As indicated in Equation (A-8), the two instantaneous phase functions, $\phi_V(t)$ and $\phi_H(t)$, are related to X(t) and Y(t) as follows:

$$\phi_V(t) = \tan^{-1}\left[\frac{Y_V(t)}{X_V(t)}\right] \tag{A-19}$$

and

$$\phi_H(t) = \tan^{-1}\left[\frac{Y_H(t)}{X_H(t)}\right] \tag{A-20}$$

where X(t) and Y(t) are as defined in Equation (A-5) and (A-6). The task at hand in this derivation is to determine the probability density function of O(t) for several clutter models.

UNIFORM PHASE CLUTTER MODEL

For the first clutter model, assume the instantaneous receive phase for each channel is uniformly distributed over 0 to 2π radians. This model is thought to be valid if the clutter is composed of many approximately equal amplitude scatterers in a common range cell. The derivation of the probability density function, $p(\phi)$, follows: Let $Z = \frac{Y}{X}$, then $\phi = \tan^{-1}(Z)$. If X and Y are each zero mean Gaussian random variables, then it can be shown that[18]

$$p(Z) = \frac{C/\pi}{(Z^2+C^2)} \quad ; \text{ all } Z \tag{A-21}$$

where

$C = \sigma_2/\sigma_1$

σ_1 = standard deviation of Y and,

σ_2 = standard deviation of X.

The probability density of ϕ is related to p(Z) as[17]

$$p_\phi(\phi) = \sec^2\phi\, p_Z(Z \to \tan\phi); \quad |\phi| \leq \pi/2 \tag{A-22}$$

or

$$p_\phi(\phi) = \frac{1}{\pi} \frac{C \sec^2\phi}{(C^2+\tan^2\phi)} \quad ; \quad |\phi| \leq \pi/2 \tag{A-23}$$

For the case of $\sigma_1 = \sigma_2$ or C = 1, Equation (A-23) becomes

$$p_\phi(\phi) = \frac{1}{\pi} \quad ; \quad |\phi| \leq \pi/2 \tag{A-24}$$

and the phase is uniformly distributed. For non-unity values of C, the phase is non-uniformly distributed about the zero value of ϕ. The difference in ϕ_V and ϕ_H is given by the convolution of $p_\phi(\phi_V)$ and $p_\phi(-\phi_H)$ as follows:

$$p_\alpha(\alpha) = p_\phi(\phi)_V \circledast p_\phi(-\phi_H) \tag{A-25}$$

where

$$\alpha = \phi_V - \phi_H$$

In general, this computation is done digitally on a computer. However, when C = 1, it is obvious that

$$p_\alpha(\alpha) = \frac{1}{\pi} \; ; \quad |\alpha| \leq \pi/2 \tag{A-26}$$

Since the phase for this this case is uniformly distributed, the detector output density function is easily determined to be

$$p_o(O) = \frac{1/\pi}{\sqrt{1-O^2}} \; ; \quad |O| \leq 1 \tag{A-27}$$

where O is the same as O(t), the detector output voltage. For non-unity values of C, $p_o(O)$ is determined with the computer digitally.

A non-fluctuating target added to the clutter signal is modeled by allowing the random variables X and Y to take on non-zero means. The density functions for O(t) then becomes more complicated. The derivation follows with:

$$Z = \frac{Y}{X},$$

$$p_X(X) = \frac{1}{\sqrt{2\pi\sigma_1^2}} \; \text{Exp} \left[-(X-a)^2/2\sigma_1^2\right]; \; \text{all } X \tag{A-28}$$

and,

$$p_Y(Y) = \frac{1}{\sqrt{2\pi\sigma_2^2}} \; \text{Exp} \left[-(Y-b)^2/2\sigma_2^2\right]; \; \text{all } Y \tag{A-29}$$

then[17]

$$p_Z(Z) = 2 \int_{\infty}^{\infty} Y p_X(ZY) p_Y(Y) \, dY \tag{A-30}$$

Substituting Equation (A-28) and (A-29) into (A-30) and completing the square in the exponent yields

$$p_Z(Z)=\text{Exp}\left\{\frac{-(bZ-a)^2}{2(\sigma_2^2Z^2+\sigma_1^2)}\right\}\int_{-\infty}^{\infty}\frac{Y}{\pi\sigma_1\sigma_2}\,\text{Exp}\left[-\frac{(AY-B)^2}{2\sigma_1^2\sigma_2^2}\right]dY \tag{A-31}$$

where

$$A=\sqrt{\sigma_2^2Z^2+\sigma_1^2} \tag{A-32}$$

$$B=\frac{\sigma_2^2aZ+\sigma_1^2b}{\sqrt{\sigma_2^2Z^2+\sigma_1^2}} \tag{A-33}$$

The value of the integral in Equation (A-31) is determined by using the identity in Reference (19) with the proper substitutions. Thus,

$$p_Z(Z)=\text{Exp}\left[\frac{-(bZ-a)^2}{2(\sigma_2^2Z^2+\sigma_1^2)}\right]\left\{\frac{\sigma_1\sigma_2}{\pi(\sigma_2^2Z^2+\sigma_1^2)}\cdot\text{Exp}\left[-\frac{(\sigma_2^2aZ+\sigma_1^2b^2)}{2\sigma_1^2\sigma_2^2(\sigma_2^2Z^2+\sigma_1^2)}\right]+\right.$$

$$\left.+\frac{(\sigma_2^2aZ+\sigma_1^2b)}{\sqrt{2\pi}(\sigma_2^2Z^2+\sigma_1^2)^{3/2}}\cdot\left[1+\text{ERF}\left(\frac{\sigma_2^2aZ+\sigma_1^2b}{\sqrt{2}\sigma_1\sigma_2\sqrt{\sigma_2^2Z^2+\sigma_1^2}}\right)\right]\right\} \tag{A-32}$$

where

a is the mean signal level of the in-phase component (with non-fluctuating target present),

b is the mean signal level of the quadrature component (with non-fluctuating target present), and

σ_1^2, σ_2^2 are the clutter levels in the two orthogonal components of the signal.

It is convenient at this point in the derivation to redefine some of the parameters in Equation (A-32). First define a voltage target-to-clutter ratio for both the in-phase and quadrature components as follows:

$$\beta_I = a/\sqrt{2\sigma_1}$$
$$\beta_Q = b/\sqrt{2\sigma_2} \qquad \text{(A-33)}$$

Then, define a clutter distribution shape factor as

$$C = \frac{\sigma_1}{\sigma_2} \qquad \text{(A-34)}$$

As is explained in Section 2, when the clutter power or variance in the in-phase and quadrature components of the receive signal are unequal, then the resultant phase probability distribution is not uniform but shaped. With the newly defined variables, the expression in Equation (A-32) becomes

$$\rho_Z(Z) = \frac{C\ \mathrm{Exp}\left[-(\beta_I^2+\beta_Q^2)\right]}{(Z^2+C^2)} + \frac{C(\beta_I Z+C\beta_Q)}{\sqrt{\pi}(Z^2+C^2)^{3/2}} \cdot \qquad \text{(A-35)}$$
$$\cdot\ \mathrm{Exp}\left[-\frac{(\beta_Q Z-\beta_I C)^2}{(Z^2+C^2)}\right] \cdot \left[1+\mathrm{ERF}\left(\frac{\beta_I Z+C\beta_Q}{\sqrt{C^2+Z^2}}\right)\right]$$

The instantaneous phase in either of the two receiver channels (H or V) is given by

$$\phi = \tan^{-1}(Z) \qquad \text{(A-36)}$$

The probability density for ϕ is related to that of Z as follows:

$$f_\phi(\phi) = (\sec^2\phi)\, p_Z(Z \rightarrow \tan\phi) \tag{A-37}$$

Making this transformation, Equation (A-35) becomes

$$f_\phi(\phi) = (\sec^2\phi)\left\{\frac{C\,\mathrm{Exp}\left[-(\beta_I^2+\beta_Q^2)\right]}{(C^2+\tan^2\phi)} + \frac{C(\beta_I\tan\phi+C\beta_Q)}{\sqrt{\pi}(C^2+\tan^2\phi)^{3/2}}\cdot\right.$$

$$\left.\cdot\,\mathrm{Exp}\left[-\frac{(\beta_Q\tan\phi-\beta_I C)^2}{(C^2+\tan^2\phi)}\right]\cdot\left[1+\mathrm{ERF}\left(\frac{\beta_I\tan\phi+C\beta_Q}{\sqrt{C^2+\tan^2\phi}}\right)\right]\right\} \tag{A-38}$$

If the polarimetric phase of the target return assumes a particular value, say 90^0, then Equation (A-38) is simplified by allowing the in-phase target-to-clutter ratio, β_I, to have zero value. Equation (A-38) then becomes

$$f_\phi(\phi) = (\sec^2\phi)\left\{\frac{C\,\mathrm{Exp}\,(\beta^2)}{(C^2+\tan^2\phi)} + \frac{C^2\beta\,\mathrm{Exp}\left[\frac{-\beta\tan^2\phi}{C^2+\tan^2\phi}\right]}{\sqrt{\pi}(C^2+\tan^2\phi)^{3/2}}\cdot\right.$$

$$\left.\cdot\left[1+\mathrm{ERF}\left(\frac{C\beta}{\sqrt{C^2+\tan^2\phi}}\right)\right]\right\} \tag{A-39}$$

To properly normalize the above equation, one must divide it by $[1 + \mathrm{ERF}(\beta)]$. This is the expression presented in Section 2 as Equation (2-8).

For the special case where the shape factor is unity, the probability density function of the detector output given by Equation (A-27) can be derived without using the computer to provide digitial convolution. The resulting density function is presented in Section 2 as Equation (2-6).

THIS PAGE IS INTENTIONALLY LEFT BLANK

REFERENCES

1. "Performance Analysis of Stationary Target Detection Techniques," 1981 Combat Identification Systems Conference, October 1981.

2. L. C. Bomar and J. D. Echard, "Evaluation of Selected Target Discrimination Techniques," Georgia Institute of Technology, Engineering Experiment Station, Atlanta, Georgia, and A. H. Green, MIRADCOM, Redstone Arsenal, Alabama at Eighth ARPA/Tri-Service Millimeter Wave Conference, 5 April 1979.

3. D. J. Lewinski, J. D. Echard, E. O. Rausch, "Stationary Target Detection and Classification Studies (U)," Final Report DELCS-TR-76-0961-F, Contract N00014-76-C-0961, Georgia Institute of Technology, Engineering Experiment Station, April 1979, UNCLASSIFIED.

4. N. F. Ezquerra and J. D. Echard, "Stationary Tactical Target Classification (U)," Non-Cooperative Target Recognition Conference, October 1979, paper UNCLASSIFIED, proceedings SECRET NOFORN.

5. J. D. Echard and N. F. Ezquerra, "Classification of Military Targets by Radar (U)," 25th Annual Tri-Service Radar Symposium, September 1979, paper CONFIDENTIAL, proceedings SECRET.

6. J. D. Echard and E. O. Rausch, Stationary Tactical Target Classification, Non-Cooperative Target Recognition Conference, October 1978, paper UNCLASSIFIED, proceedings SECRET.

7. E. K. Reedy, J. L. Eaves, S. O. Piper, W. K. Parks, S. P. Brookshire, R. D. Wetherington, and R. N. Trebits, Stationary Target Detection and Classification Studies (U), Second Interim Report ECOM-76-0961-2, Contract N0014-76-C-0961, Georgia Institute of Technology, Engineering Experiment Station, March 1978, CONFIDENTIAL.

8. E. K. Reedy, J. L. Eaves, S. O. Piper, W. K. Parks, N. T. Alexander, and B. O. Pyron, Stationary Target Detection and Classification Studies (U), Semi-Annual Report ECOM-76-0961-1, Contract N00014-75-C-0320, Mod. P00003, Georgia Institute of Technology, Engineering Experiment Station, August 1976, CONFIDENTIAL, ADC009943L.

9. B. Gelernter, W. Johnson, E. K. Reedy, J. L. Eaves, S. O. Piper, W. K. Parks, and S. P. Brookshire, "Stationary Target Discrimination and Classification Studies (U)," 23rd Annual Tri-Service Radar Symposium, July 1977, paper CONFIDENTIAL, proceedings SECRET.

10. S. O. Piper and E. O. Rausch, Detection and Classification Techniques Investigation, Non-Cooperative Target Recognition Conference, November 1977, CONFIDENTIAL.

REFERENCES

(continued)

11. B. O. Pyron and M. C. McGee, Stationary Ground Target Radar Detection and Classification Bibliography (U), Volume I, Final Report ECOM-76-0961-B1, Contract N00014-76-C-0961, Georgia Institute of Technology, Engineering Experiment Station, February 1978, UNCLASSIFIED.

12. B. O. Pyron and M. C. McGee, Stationary Ground Target Radar Detection and Classification Biblography (U), Volume II, Final Report ECOM-76-0961-B2, Contract N00014-76-C-0961, Georgia Institute of Technology, Engineering Experiment Station, February 1978, CONFIDENTIAL.

13. B. O. Pyron and M. C. McGee, Stationary Ground Target Radar Detection and Classification Bibliography (U), Volume III, Final Report ECOM-76-0961-B3, Contract N00014-76-C-0961, Georgia Institute of Technology, Engineering Experiment Station, Feburary 1978, SECRET.

14. D. J. Lewinski, E. O. Rausch, S. O. Piper, and J. L. Eaves, Stationary Target Detection and Classification Studies (U), Final Report ERADCOM-76-0961-F, Contract N00014-76-C-0961, Georgia Institute of Technology, Engineering Experiment Station, May 1978, UNCLASSIFIED.

15. J. D. Echard, J. A. Scheer, E. O. Rausch, W. H. Licata, J. R. Moore, and J. A. Nestor, "Radar Detection, Discrimination and Classification of Buried Non-Metallic Mines," Final Technical Report, USA MERADCOM, Contract DAAG53-76-C-0112, Georgia Institute of Technology, Engineering Experiment Station, February 1978, UNCLASSIFIED.

16. H. M. Finn and R. S. Johnson, "Adaptive Detection Mode With Threshold Control As A Function Of Spatially Sampled Clutter-Level Estimates," RCA Review, September 1978.

17. A. Papoulis, Probability, Random Variables and Stochastic Processes, McGraw-Hill Book Company, New York, 1965, Chapters 5 and 7.

18. J. Omura and T. Kailath, "Some Useful Probability Distributions," Technical Report No. 7050-6, Stanford Electronics Laboratories, Stanford University, September 1965, pp. 86-92.

19. I. S. Gradshteyn and I. M. Ryzhik, Table of Integrals, Series, and Products, Academic Press, New York, NY, 1965.